Title
THE PHOTOCHEMISTRY OF N03 AND THE KINETICS OF THE N2O[--O, SYSTEM

Author
Graham, Richard A.

Publication Date
1977-05-01

Submitted to Journal of Physical Chemistry

LBL-6276
Preprint c.1

THE PHOTOCHEMISTRY OF NO_3 AND THE KINETICS OF THE N_2O_5-O_3 SYSTEM

Richard A. Graham and Harold S. Johnston

May 1977

Prepared for the U. S. Energy Research and Development Administration under Contract W-7405-ENG-48

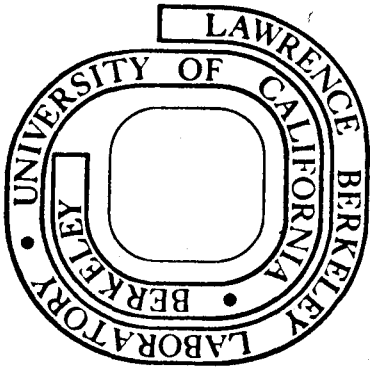

DISCLAIMER

LBL-6276

The Photochemistry of NO_3 and the Kinetics of the N_2O_5-O_3 System

By

Richard A. Graham and Harold S. Johnston

Department of Chemistry and Materials and Molecular Research Division, Lawrence Berkeley Laboratory, University of California, Berkeley, California 94720

Abstract

The kinetics of the nitrogen pentoxide catalyzed decomposition of ozone were studied in the dark and with photolytic light absorbed by the NO_3 radical. Ultraviolet, visible, or infrared absorption cross sections were measured for N_2O_5, HNO_3, NO_2, and NO_3 in this study. The equilibrium constant for $N_2O_5 \rightleftharpoons NO_2 + NO_3$ was found to be: (molecules cm^{-3}, 298-329 K)

$$K = (8.4 \pm 1.8) \times 10^{26} \exp[-(11180 \pm 100)/T]$$

The rate constants for several reactions were measured: (cm^3 $molecule^{-1}$ sec^{-1})

$2\ NO_3 \rightarrow 2\ NO_2 + O_2$	$g = (8.5 \pm 2.8) \times 10^{-13} \exp[-(2450 \pm 100)/T]$
$O + N_2O_5 \rightarrow$ products	$m \leq 2 \times 10^{-14}$
$O + NO_3 \rightarrow O_2 + NO_2$	$n = (1.0 \pm 0.4) \times 10^{-11}$

By combining the equilibrium constant K with literature values[3,36] of Ke and Kf, rate constants for reactions e and f were evaluated:

$NO_2 + NO_3 \rightarrow NO + O_2 + NO_2$	$e = (2.5 \pm 0.5) \times 10^{-14} \exp[-(1230 \pm 100)/T]$
$NO + NO_3 \rightarrow 2\ NO_2$	$f = (1.9 \pm 0.4) \times 10^{-11}$ at 297 K

At one atmosphere total pressure, the photolysis of NO_3 occurs with a primary quantum yield less than one in the red region of the spectrum. Under tropospheric conditions with an overhead sun, the solar photolysis constants at 298 K for the two paths of dissociation were found to be:

$NO_3 + h\nu \rightarrow NO + O_2$	$j_1 = 0.040 \pm 0.02\ sec^{-1}$
$NO_3 + h\nu \rightarrow NO_2 + O$	$j_2 = 0.099 \pm 0.02\ sec^{-1}$

The average quantum yield for process two was approximately 0.77 for light with wavelengths between 470 and 610 nm, and that for process one was about 0.23 between 470 and 610 nm but only 0.07 in the strong absorption region between 610 and 670 nm. The photolysis constants may be larger at lower total pressures.

Errors made in previous studies in this laboratory[23,25] are corrected: reported cross sections for the near ultraviolet absorption by HNO_2 were much too low; an infrared absorption ascribed to NO_3 is due to N_2O_5; previously reported visible cross sections for NO_3 were found to be about a factor of four too low and are corrected here; previously reported ultraviolet cross sections for N_2O_5 are revised slightly.

I. Introduction

The interactions of the higher oxides of nitrogen and ozone provide a classic case wherein complex laboratory reactions are explainable in terms of sets of elementary reactions.[1] Conversely, the rate constants of the elementary reactions are evaluated by combining data from several different laboratory systems. The complex reactions are: I. the thermal decomposition of nitrogen pentoxide;[2-4] II. the reaction of nitrogen pentoxide and nitric oxide;[5-11] III. the formation of nitrogen pentoxide from nitrogen dioxide and ozone;[12-16] IV. the nitrogen pentoxide catalyzed decomposition of ozone.[17-20]

$$\text{I.} \quad 2\ N_2O_5 \rightarrow 4\ NO_2 + O_2$$

$$\text{II.} \quad N_2O_5 + NO \rightarrow 3\ NO_2$$

$$\text{III.} \quad 2\ NO_2 + O_3 \rightarrow N_2O_5 + O_2$$

$$\text{IV.} \quad 2\ O_3 + N_2O_5 \rightarrow 3\ O_2 + N_2O_5$$

These four complex reactions are explained quantitatively by six elementary chemical reactions involving the nitrate free radical, NO_3.[1]

The photochemistry of NO_3 is potentially important in the balance of ozone in the troposphere and lower stratosphere.[21] If the photolysis products are nitric oxide and oxygen, the net effect is catalytic destruction of ozone:

$$NO_3 + h\nu \rightarrow NO + O_2$$

$$NO + O_3 \rightarrow NO_2 + O_2$$

$$NO_2 + O_3 \rightarrow NO_3 + O_2$$

$$\text{net:} \quad 2\ O_3 + h\nu \rightarrow 3\ O_2$$

If the photolysis products are nitrogen dioxide and atomic oxygen, there is no net chemical reaction:

$$NO_3 + h\nu \rightarrow NO_2 + O$$
$$O + O_2 + M \rightarrow O_3 + M$$
$$NO_2 + O_3 \rightarrow NO_3 + O_2$$

net: null reaction

The primary goal of this study was to obtain the primary quantum yields for the photolysis of NO_3. As a part of the study, it was necessary to determine the optical absorption spectra of several oxides and oxyacids of nitrogen and the rate constants of several elementary reactions.

Jones and Wulf[22] used photographic spectroscopy to obtain the low absorption cross sections of nitrogen pentoxide between 285 and 390 nm at room temperature, and some results for 210 to 290 nm were previously reported from this laboratory.[23] Ramsay[24] studied the visible NO_3 spectrum under high dispersion and concluded that the observed diffuseness indicates predissociation. He identified a short progression in the symmetric stretching vibration of NO_3 beginning with the strong zero-zero transition at 662 nm and extending to shorter wavelengths with approximately 950 cm^{-1} intervals to 559 nm. At least 15 other bands in the visible region are unassigned. Visible cross sections for NO_3 were measured by Schott and Davidson[4] at high temperature in a shock tube, and they found the absorption spectrum to change with temperature. The only report of an infrared NO_3 absorption is a weak band between 1325 and 1375 cm^{-1} observed in an N_2O_5-O_3 system by Cramarossa and Johnston.[25] Nitric acid vapor is often a by-product of nitrogen pentoxide in laboratory

apparatus; its ultraviolet spectrum has been studied,[26-30] and nitric acid has been measured in the atmosphere by way of its infrared absorption spectrum.[31,32]

Neither the reaction rate nor products of the reaction of atomic oxygen with nitrogen pentoxide are known, but Murphy[33] derived an upper limit of 8×10^{-14} cm^3 $molecule^{-1}$ sec^{-1} from NO_2 photolysis in the presence of N_2O_5. No rate constant has been reported for the reaction of oxygen atoms with NO_3. The only experimentally determined value for the equilibrium constant, K, for the reaction

$$N_2O_5 \rightleftharpoons NO_2 + NO_3$$

$$K = [NO_2][NO_3]/[N_2O_5]$$

appears to be that of Schott and Davidson[4] from shock-tube pyrolysis of N_2O_5 between 450 and 550 K.

Although N_2O_5-O_3 kinetics have been cited as an example of a well understood complex mechanism,[34,35] further study of these reactions seemed to be needed. In the present study, several different experimental quantities were measured. Conventional spectroscopic methods were used to obtain absorption cross sections for various oxides and oxyacids of nitrogen. To obtain absolute cross sections for the NO_3 absorption spectrum, simultaneous molecular modulation measurements were made for NO_3 and N_2O_5 since the formation of one was primarily caused by the disappearance of the other in the system used. Four other photochemical and chemical kinetic studies were made: (1) The rate constant for the reaction between nitrogen dioxide and ozone.[14] (2) The steady-state concentration of the NO_3 radical in the presence of N_2O_5 and O_3.

(3) The rate constant for the N_2O_5 catalyzed decomposition of ozone, with and without photolytic illumination of NO_3. (4) The amplitude and phase shift of the molecular modulation of NO_3 with either oxygen or nitrogen as buffer gas and irradiation by red, gold, or green fluorescent lamps.

II. Mechanism

The experimental data were interpreted in terms of the following 15 step chemical mechanism:

$$\left.\begin{aligned} N_2O_5 &\xrightarrow{A(M)} NO_2 + NO_3 \\ NO_2 + NO_3 &\xrightarrow{B(M)} N_2O_5 \end{aligned}\right\} K = \frac{A(M)}{B(M)} \qquad (1)$$

$$NO_2 + NO_3 \xrightarrow{e} NO + O_2 + NO_2$$

$$NO + NO_3 \xrightarrow{f} NO_2 + NO_2$$

$$NO_3 + NO_3 \xrightarrow{g} NO_2 + NO_2 + O_2$$

$$NO_2 + O_3 \xrightarrow{h} NO_3 + O_2$$

$$NO + O_3 \xrightarrow{i} NO_2 + O_2$$

$$NO_3 + h\nu \text{ (vis.)} \xrightarrow{j_1} NO + O_2$$

$$NO_3 + h\nu \text{ (vis.)} \xrightarrow{j_2} NO_2 + O$$

$$N_2O_5 + O \xrightarrow{m} \text{products}$$

$$NO_3 + O \xrightarrow{n} NO_2 + O_2$$

$$O_3 + h\nu \text{ (vis.)} \xrightarrow{p} O_2 + O$$

$$O_3 + O \xrightarrow{q} O_2 + O_2$$

$$O + O_2 + M \xrightarrow{r} O_3 + M$$

$$NO_3 \text{ on walls} \xrightarrow{w} NO_2 + 1/2\ O_2$$

For the simplified mechanism using reactions *A*, *B*, *g*, and *h*, the steady-state NO_3 concentration and the rate of destruction of ozone is given exactly by the following expressions[17,1]

$$[NO_3]_{ss} = (Kh/2g)^{1/3}[N_2O_5]^{1/3}[O_3]^{1/3} \quad (2)$$

$$-\frac{1}{2}\frac{d[O_3]}{dt} = \frac{1}{2}(Kh)^{2/3}(2g)^{1/3}[N_2O_5]^{2/3}[O_3]^{2/3} \quad (3)$$

The full mechanism without light, reactions *A* through *i* plus *w*, involves more complex expressions, but they can be solved by a process of successive approximation for $[NO_3]$:

$$[NO_3]_{ss} = \left(\frac{Kh}{2g}\right)^{1/3}[N_2O_5]^{1/3}[O_3]^{1/3}\ \alpha^{1/3} \quad (4)$$

$$\alpha = \left(1 - \frac{\beta e}{h}\frac{[NO_3]}{[O_3]} - \frac{w}{Kh}\frac{[NO_3]^2}{[O_3][N_2O_5]}\right) \quad (5)$$

$$\beta = \frac{2f[NO_3] + i[O_3]}{f[NO_3] + i[O_3]} \quad (6)$$

$$-\frac{1}{2}\frac{d[O_3]}{dt} = \frac{1}{2}(Kh)^{2/3}(2g)^{1/3}(\alpha)^{-1/3}[N_2O_5]^{2/3}[O_3]^{2/3} \quad (7)$$

Measurements of the steady-state concentration of NO_3 and the rate of ozone decomposition in the presence of N_2O_5 yield two quantities, $(Kh/2g)^{1/3}\ \alpha^{1/3}$ and $\frac{1}{2}(Kh)^{2/3}(2g)^{1/3}\ \alpha^{-1/3}$, whose product is $\frac{1}{2}Kh$. From the independently measured[14] rate constant *h*, the values of *K* and *g* are found. From literature values[3,36] for *Ke* and *Kf*, the values of *e* and *f* can be calculated, and the literature value[37] for *i* then provides enough data to evaluate all terms in α and β except the one involving *w*. Equations 4 and 5 can be rewritten as

$$\left\{\frac{[NO_3]^3}{[O_3][N_2O_5]} + \left(\frac{Kh}{2g}\right)\frac{e}{h}\beta\frac{[NO_3]}{[O_3]}\right\}_{i-1} = \left(\frac{Kh}{2g}\right)_i - \left(\frac{w}{2g}\right)_i\frac{[NO_3]^2}{[O_3][N_2O_5]} \quad (8)$$

By plotting the left-hand-side of Equation 8 against $[NO_3]^2/[O_3][N_2O_5]$, one obtains $(w/2g)$ as the slope and $(Kh/2g)$ as the intercept. The process is reiterated. Since the effect of reactions e, f, i, and w on the data evaluation was typically less than 10 percent, this process of successive approximation quickly converges on final values for the rate constants.

When visible light absorbed by NO_3 is passed through the reaction vessel containing N_2O_5 and ozone, the steady-state concentration of NO_3 and the rate expression for ozone decay have the following form:

$$[NO_3]_{ss} = \left(\frac{Kh}{2g}\right)^{1/3} [O_3]^{1/3} [N_2O_5]^{1/3} \gamma^{1/3} \tag{9}$$

$$\gamma = \left(1 - \frac{\delta e}{h}\frac{[NO_3]}{[O_3]} - \frac{w}{Kh}\frac{[NO_3]^2}{[O_3][N_2O_5]} - \frac{j_1 + j_2}{Kh}\frac{[NO_3]^2}{[O_3][N_2O_5]}\right) \tag{10}$$

$$\delta = \beta + \frac{f[NO_3]\, j_1[NO_3]}{Ke[N_2O_5]\{f[NO_3] + i[O_3]\}} \tag{11}$$

$$-\frac{1}{2}\left\{\frac{d[O_3]}{dt} - j_2[NO_3] + j_1(2-\beta)[NO_3]\right\} \tag{12}$$

$$= \frac{1}{2}(Kh)^{2/3}(2g)^{1/3}\gamma^{-1/3}[N_2O_5]^{2/3}[O_3]^{2/3}$$

The net observed photolysis constant for NO_3 is $(j_2 + \beta j_1)$. These expressions apply for the case of excess oxygen, where the concentration of oxygen atoms is suppressed.

The photolysis constant for NO_3 is derived from the behavior of a N_2O_5-O_3 steady state flow system with the photolysis lamps being

turned on and off by a low frequency square wave. Since the concentrations of the chemical species vary periodically in time due to the photolysis lamps, they can be described by a Fourier series of the form

$$F(\omega t) = C_o + \sum_{n=1}^{\infty} C_n \sin\left(n\omega t + \delta_n\right) \tag{13}$$

where $\omega = 2\pi f$, f is the flashing frequency, the C_n are the amplitudes, and the δ_n are the phase shifts. The flashing lamps are represented by a square wave

$$L(\omega t) = \frac{I}{2} + \frac{2I}{\pi} \sum_{\substack{\text{odd} \\ n}}^{\infty} \frac{1}{n} \sin(n\omega t) \tag{14}$$

where $\delta_n = 0$. The values for δ_n for the other chemical species are their phase shifts relative to the photolysis lamps.

A system using red lamps for photolysis is used here for an illustrative calculation. Red light has insufficient energy for reaction j_2 to occur, and the importance of the oxygen atom reactions n and m can be suppressed by using oxygen as the carrier gas. Reactions e, f, i, and w have less than a 10 percent effect on the NO_3 concentration and are neglected in order to simplify the reaction set. The differential equation for NO_3 is then given by:

$$\begin{aligned} \frac{d[NO_3]}{dt} &= A[N_2O_5] - B[NO_2][NO_3] \\ &\quad - 2g[NO_3]^2 + h[NO_2][O_3] + \frac{F}{V}\left([NO_3]_{in} - [NO_3]_{out}\right) \\ &\quad - [NO_3]\left[\frac{j_1}{2} + \frac{2j_1}{\pi} \sum_{\substack{\text{odd} \\ n}}^{\infty} \frac{1}{n} \sin(n\omega t)\right] \end{aligned} \tag{15}$$

where F = flow rate.

V = volume of cell.

$[NO_3]_{in}$ = concentration of NO_3 flowing into the cell.

$[NO_3]_{out}$ = concentration of NO_3 flowing out of the cell.

j_1 = wavelength integrated product of the light intensity, NO_3 absorption cross section, and primary quantum yield.

The low quantum yield of red light photolysis results in periodic changes in $[NO_3]$ that are much less than one percent. In this system NO_2 is a low concentration, fast intermediate compared to NO_3, and an approximate steady state expression for NO_2 is

$$[NO_2] = \frac{1}{B[NO_3] + h[O_3]} \left\{ A[N_2O_5] + 2g[NO_3]^2 + [NO_3] \left[\frac{j_1}{2} + \frac{2j_1}{\pi} \sum_{\substack{\text{odd} \\ n}}^{\infty} \frac{1}{n} \sin(n\omega t) \right] \right\} \tag{16}$$

This expression is substituted into Equation 15 to give:

$$\frac{d[NO_3]}{dt} = \frac{2}{B[NO_3] + h[O_3]} \left\{ A[N_2O_5]\ h[O_3] - B[NO_3]\ 2g[NO_3]^2 - B[NO_3]^2 \left[\frac{j_1}{2} + \frac{2j_1}{\pi} \sum_{\substack{\text{odd} \\ n}}^{\infty} \frac{1}{n} \sin(n\omega t) \right] \right\} + \frac{F}{V} \left([NO_3]_{in} - [NO_3]_{out} \right) \tag{17}$$

Since $B[NO_3] \geq 10\ h[O_3]$ under typical experimental conditions at 298 K and one atmosphere pressure, the $h[O_3]$ term in the denominator of Equation 17 will be neglected. For a system at steady state with respect to products

and reactants, the unmodulated terms in Equation 17 cancel out. Only the modulated or AC terms are left, and the expression for the modulation of the NO_3 concentration by the flashing lamps is:

$$\frac{d[NO_3]}{d\theta_{AC}} = -2[NO_3]\left[\frac{j_1}{\pi^2 f}\sum_{\substack{\text{odd}\\ n}}^{\infty}\frac{1}{n}\sin(n\theta)\right] \tag{18}$$

where $\theta = \omega t$.

Since the modulation of the NO_3 concentration is less than one percent, $[NO_3]$ will be essentially constant and Equation 18 integrates in closed form to give:

$$[NO_3]_{AC} = 2[NO_3]\left[\frac{j_1}{\pi^2 f}\sum_{\substack{\text{odd}\\ n}}^{\infty}\frac{1}{n^2}\cos(n\theta)\right] \tag{19}$$

Hence, the concentration modulation of NO_3 is a triangular wave with a phase shift of +90° referred to the flashing lamps (Equation 14). The modulation amplitude is directly proportional to the light intensity and the primary quantum yield. Only the first term of the series in Equation 19 is used since the experimentally measured quantities are the phase shift and amplitude of the first harmonic of the modulation signal. The above mathematical treatment represents an approximation; the actual data analysis uses the complete kinetic mechanism and is performed by a computer program using the Gear method.[38]

Ground state oxygen atoms (O^3P) are generated in the N_2O_5-O_3 system from photolysis of both O_3 and NO_3. Because atomic oxygen is a very fast intermediate, reactions *m* and *n* would result in a NO_3 modulation with the same phase shift as the NO_3 photolysis reactions. Nitrogen was used

as a carrier gas in experiments to measure the rate constants for reactions *m* and *n*. A low, known concentration of oxygen was present due to a small amount of oxygen in helium flowing through the ozonizer. Since the rate of reaction *r*, $O + O_2 + M$, is about 10 times that of any other oxygen atom reaction, the oxygen atom concentration is almost directly proportional to the rate constant for this reaction and can be readily calculated. The modulation contributions from reactions *m* and *n* can then be separated by varying the NO_3 to N_2O_5 ratio.

III. Experimental

A. Reaction Cells

A diagram of the experimental apparatus is presented in Figure 1. The reaction cell is a cylindrical quartz tube, 15 cm in diameter and 178 cm long. The quartz tube is O-ring sealed to two nickel-plated stainless steel end caps; all O-rings are made of silicone rubber. The end caps are 18 cm and 24 cm long and are mounted in a rigid steel frame. The volume of the cell is 45.3 liters and the surface to volume ratio is 2.5 cm^{-1}. Three aluminum coated, 8.6 cm diameter mirrors are mounted in the end caps to give multiple reflections: optical paths of 861, 1717, 2573, and 3429 cm can be selected by an external adjustment screw. Calcium fluoride windows transmit radiation from the far-ultraviolet to approximately 9.5 microns in the infrared. The reaction cell can be evacuated to less than 10^{-3} torr by a liquid nitrogen trapped oil diffusion pump. The cell and optical train are mounted on a Newport Research Corporation vibration isolation table.

The gas cell is enclosed in an insulated box with walls of six inch thick urethane boards faced with one inch coated fiberglass boards. The light beam enters through evacuated glass tubes sealed with calcium fluoride windows. Cooled methanol from a Neslab LT-9 circulator or chilled water is pumped into an elevated 22 liter surge tank. The coolant then flows through a finned gravity coil mounted on top of the reaction cell frame, and a blower circulates air around the coil. The temperature of the cell is regulated by a contact thermometer and relay operating a heating wire wrapped around the cooling coil. Experiments can be

performed between 233 and 343 K. Six iron-constantan thermocouples mounted around the cell and a thermocouple inside a six-inch stainless steel thermowell in the cell indicated a temperature homogeneity of ± 0.2 K with the lamps flashing.

A similar reaction cell[39] was also used for monitoring the decay of ozone in the presence of nitrogen pentoxide and for modulation experiments to determine the absorption cross sections for NO_3. A quartz tube 29 cm in diameter and 91 cm long is O-ring sealed to nickel-plated stainless steel end caps to give a 67.0 liter volume and a 1.8 cm^{-1} surface-to-volume ratio. Optical path lengths between 4 and 32 meters can be obtained with the gold-coated multiple reflection mirrors. A Nernst glower is the infrared source and KBr windows are used. The temperature control, electronics, detectors, monochromator, and gas handling system used with this system (IR cell) are identical with the ones that will be described for the primary reaction cell (UV cell).

B. Detection System

Three light sources are used with the main reaction cell: a Sylvania DE450A deuterium arc lamp is used for UV work and a tungsten lamp for the visible region, one of these two being mounted next to an American Time Products 400 cps tuning fork chopper; a Nernst glower for the infrared region with its own 400 cps tuning fork can be used as the source beam by turning one mirror. The source beam passes through the reaction cell and then to a McPherson Model 2051 1-m grating monochromator with a 150 line/mm grating and order sorting filters for infrared spectroscopy and a 1200 line/mm grating and colored glass filters for visible and ultraviolet work. The infrared detector is a Santa Barbara

Research Center copper-doped germanium photoconductor cooled to liquid helium temperature (4 K). An EMI 9526B photomultiplier for ultraviolet spectroscopy and a RCA 4832 photomultiplier for the visible region are biased by a Fluke Model 408B power supply. The infrared detector and one of the photomultipliers are mounted on the two exit slits of the 1-m monochromator; turning one mirror diverts the monochromator's output from one detector to the other.

As the source beam passes through the cell, it is amplitude modulated with the flashing frequency f of the photolysis lamps at wavelengths where the reaction species absorb radiation. The modulation information is carried at the sideband frequencies 400 ± f and extracted with lock-in amplification techniques.[40,41] The higher harmonics of the f cps signal are reduced by the lock-in and filters to less than two percent of the fundamental. The system is calibrated by applying a signal of known amplitude and zero phase shift to the initial amplification stages.

A PDP 8/E minicomputer with a programmable clock was interfaced to a multiplexer and a Preston X-Mod 723A digital voltmeter with an accuracy of 1 part in 20,000 and a maximum sampling rate of 100 hertz. Spectra stored in the computer's memory can be displayed on an oscilloscope, plotted on a X-Y recorder, or stored on a dual drive Dectape unit. The modulation signals were simulated with a chemical kinetics program by Whitten.[43] This program uses the Gear[38] method for solving coupled differential equations and is run on Lawrence Berkeley Laboratory's CDC 7600 computer.

C. Photolysis Lamps

The photolytic light for these experiments was provided by red, gold, or green 30 watt General Electric F30T8 fluorescent lamps. Two of the 36 inch lamps were placed along each side of the cell with an Alzac reflector. The lamp electrodes were heated by six volt transformers to insure rapid firing. They were switched on and off by a 700 volt regulated power supply controlled by the in-phase square wave of a low frequency reference generator. The light intensity was monitored by a phototransistor to detect changes due to lamp aging; this signal showed that the lamp output was a square wave with an initial spike containing less than .01 percent of the total area at 1 hertz.

To obtain the spectral distribution of the lamps, the spectral response of the UV cell's optical system was calibrated with a General Electric 30A/T24/17 tungsten ribbon lamp. The brightness temperature of the tungsten ribbon was measured with a Leeds and Northrup Model 8622-C optical pyrometer which was calibrated at the Lawrence Berkeley Laboratory. The spectrum of the tungsten ribbon lamp was scanned from 280 to 900 nm at brightness temperatures of 2100 ± 1 K and 2173 ± 1 K (true temperatures[44] of 2300 K and 2388 K). Correction curves for the optical system were obtained by dividing the observed lamp spectra by the calculated intensity distribution, using the emissivities of DeVos.[45] When normalized at one point, the two correction curves agreed with a one percent average uncertainty.

Photolysis lamps of various colors were then used as the light source, and their spectra were recorded. The corrected photolysis lamp

spectra are presented in Figure 2. The ratios of the total photon fluxes for the green, gold, and red lamps were 1.0 : 0.56 : 0.23, respectively. The visible spectra of NO_3 and O_3 are included in Figure 2 to show the degree of overlap with the various lamps.

The average cross section for NO_3 or O_3 absorption for each lamp spectrum is the wavelength integrated product of cross section (σ_λ) and lamp intensity (I_λ):

$$\sigma_{avg}(NO_3) = \frac{\int \sigma_\lambda(NO_3)\ I_\lambda\ d\lambda}{\int I_\lambda\ d\lambda} \qquad (20)$$

The products of ozone photolysis by light in the 570 to 630 nm region are ground state oxygen atom and oxygen, and no energy chains that destroy ozone have been observed.[46,47] Since the rate constants for oxygen atom reacting with O_2 and O_3 are well known,[37] ozone can be used for actinometry with the photolysis lamps.

Ozone from a silica gel trap was liquified and pumped on to remove oxygen before being allowed to vaporize slowly into the evacuated cell to a pressure of 2 to 3 torr. Concentration determinations were made from ozone's visible absorption spectrum before and after 30 minute periods of illumination by the flashing lamps. Since 30 percent of the cell volume was in the end caps and shielded from the lamps, the actual intensity of the lamps was a factor of 1/.70 larger than that calculated from ozone destruction. The path lengths used for modulation calculations were multiples of 708 cm, the part of the monitoring beam's path that was illuminated by the lamps. After a period of illumination, up to 20 minutes were required for the ozone concentration to equalize throughout

the cell. Ozone measurements in the dark cell were made during the 30 minutes after a photolysis period so that an extrapolation could be made back to the time when the lamps were turned off. Since less than 25 percent of the initial ozone was destroyed in an experiment, the average quantum yield for ozone photolysis was ≥ 1.99.

The light intensities measured for the main reaction cell were:

Lamp	297.8 K	329.0 K
Green	1.55 ± 0.15	2.03 ± 0.21
Gold	1.07 ± 0.02	
Red	0.33 ± 0.04	0.29 ± 0.05

(units are 10^{16} photons cm^{-2} sec^{-1}) (21)

Both ozone's low visible absorption cross section and the concentration fluctuations due to the end caps were responsible for the large uncertainties in the light flux measurements. The ratios of the 298 K intensities for the green, gold, and red lamps (1.0 : 0.69 : 0.21) are similar to those obtained from spectral distribution measurements of the lamps when they were new.

D. Gases and Flow System

The purification of nitrogen dioxide and the preparation of nitric acid have been previously described.[28] Ozone, prepared by electric discharge through purified oxygen,[23] was used in the 1 atm flow system or collected on 6 to 12 mesh silica gel at 193 K for actinometry or for later desorption by a N_2 carrier gas into the flow system. The glass manifold for handling the gases used stainless steel Cajon ultra-torr

fittings and greaseless Teflon stopcocks with Viton O-rings and was evacuated by a liquid nitrogen trapped oil diffusion pump. A Texas Instruments Model 145 quartz spiral manometer was used to measure gas pressures.

The carrier gases for the flow experiments were provided by Lawrence Berkeley Laboratory. High dry grade nitrogen was passed through a Matheson particulate filter and through a column containing P_2O_5-coated glass beads in order to remove moisture. High dry oxygen flowed through a silica tube containing copper turnings at 900 K to convert hydrocarbons to CO_2 and H_2O and then through ascarite and P_2O_5 columns to remove these oxidation products. Extra pure helium was used without further purification. A tank of NO_2 in N_2 from Matheson Company, analyzed by ultraviolet spectroscopy to contain 812 ± 9 ppm NO_2 and 43 ± 1 ppm NO, and a tank of 0.65 percent NO_2 in N_2 prepared in this laboratory were used in flow experiments.

The flow rates of the gases into the reaction cell were measured with Manostat Predictability flowmeters or Hastings mass flowmeters, both being calibrated for the gases used by an American Meter Company wet test flowmeter. The gases were mixed and jetted into the reaction cell through a glass disperser tube. This tube lay in the bottom of, and ran the length of the reaction cell. The disperser tube had holes spaced an inch apart and sized to give approximately equal throughput at the typical operating condition of 4000 cm^3 per minute. The gases left the cell through a similar tube located at the top of the cell. The pressure drop through the cell at one atmosphere flow conditions was approximately 4 torr. Atmospheric pressure was measured by a mercury barameter to be 756 ± 2 mm Hg (0°C).

IV. Results

A. Absorption Cross Sections

The absorption cross sections and concentration measurements in the various spectral regions were obtained with the following instrument setting: UV and visible -- 0.83 nm resolution, 50 nm min^{-1} scan, 0.3 sec time constant, data collected at 0.2 sec intervals; IR — 13 nm resolution, 1.0 sec time constant, 400 nm min^{-1} scan, data collected at 0.2 sec intervals, one atmosphere total pressure. The absorption cross section σ (cm^2 $molecule^{-1}$) at the average wavelength λ is defined by

$$A \equiv \log_e I_o(\lambda)/I(\lambda) = \sigma(\lambda)\ CL \qquad (22)$$

where C is concentration in molecules cm^{-3}, L is optical path in cm, I_o is the intensity of the incident beam, and I that of the transmitted beam. A low pressure mercury lamp and the 486 nm deuterium line were used for wavelength calibration.

1. Ozone

Ozone from a silica gel trap was liquified and pumped on to remove oxygen. It was then vaporized slowly into the evacuated gas cell to a pressure of 2 to 3 torr as measured by the quartz spiral manometer. From the ozone visible cross sections of Griggs,[48] the ozone decomposition during transfer to the gas cell was determined to be one percent. The visible absorption band obeyed Beer's law and was independent of pressure between 2 torr and 1 atm and of temperature between 298 K and 329 K. Ozone concentrations in actinometry experiments were measured by averaging three data points at each of the two absorption maxima and

using a σ (574.6 nm) of 4.78×10^{-21} and a σ (602.5 nm) of 5.17×10^{-21} cm^2 $molecule^{-1}$. The ozone cross sections at the 4.72 and 4.78 μ infrared peaks were based on concentrations determined from the ozone spectrum in the visible region. The infrared ozone cross sections decreased a few percent from 298 to 329 K and varied quadratically with the observed optical density.[42]

2. Nitrous Acid

Concentrations of nitrous acid vapor prepared from mixtures of NO, NO_2, and H_2O were calculated from thermochemical data[49,50] for the equilibrium

$$NO + NO_2 + H_2O = 2\ HNO_2 \qquad (23)$$

It has since been found that the actual amount of HNO_2 was much less than the equilibrium amount, and the previously reported[23] cross sections from this laboratory were too low — perhaps by a factor of 3 to 6. Ultraviolet cross sections for HNO_2 reported by Cox and Derwent[51] are a factor of 5 to 6 higher than the earlier work.[23]

3. Nitrogen Dioxide

The ultraviolet absorption spectrum of nitrogen dioxide at room temperature obtained as a part of these studies has been published elsewhere.[23] Tanks of NO_2 in N_2 were calibrated from NO_2 cross sections in the visible region and were used in the determination of the 8 μ HNO_3 and N_2O_5 infrared cross sections. Ultraviolet cross sections reported by Bass et al.[52] are approximately 10 percent lower in the 400 nm region, but the two studies show agreement within the limits of the experimental uncertainties.

4. Nitrogen Pentoxide and Nitric Acid

Nitrogen pentoxide was prepared from O_3 and NO_2 in a one atmosphere flow system, and the concentrations of N_2O_5, HNO_3, and O_3 (all of which absorb in the ultraviolet region) were determined from their infrared absorptions. The nitric acid was apparently formed by a heterogeneous reaction on the cell walls of the N_2O_5 with ppm concentrations of H_2O in the carrier gas. According to Morris and Niki,[53] the reaction of water with N_2O_5 to give HNO_3 has a gas phase reaction rate of less than 1.3×10^{-20} at 298 K. The fast heterogeneous reaction they also observed is probably the cause of nitric acid formation in the present system. For conditions of very low ozone concentration, an appreciable amount of NO_2 is also present and can be measured by its near ultraviolet spectrum. Six ultraviolet spectra were taken with N_2O_5 concentrations of $(3\text{-}10) \times 10^{14}$ molecules cm^{-3}. The absorptions due to O_3, HNO_3, and NO_2 were subtracted from the spectra; the main source of uncertainty was the measurement of small ozone concentrations. The average uncertainty in Table I and Figure 3 is approximately 10 percent for 205 to 260 nm and 20 percent for longer wavelengths.

The N_2O_5 and HNO_3 infrared cross sections were measured in a steady state flow system using a calibrated tank of NO_2 in N_2. The N_2O_5 to HNO_3 ratio was varied by changing the amount of water vapor in the system. The cross sections were then determined by a mass balance from the HNO_3, N_2O_5, and NO_3 absorptions. The Beer-Lambert law was obeyed for optical densities less than 2.5 at the peak of the 8.03 μ Q-branch of N_2O_5:

$$\sigma(298\ K) = (1.75 \pm 0.01) \times 10^{-18}$$
$$\sigma(313\ K) = (1.68 \pm 0.02) \times 10^{-18} \qquad (24)$$
$$\sigma(329\ K) = (1.56 \pm 0.03) \times 10^{-18}$$

(Uncertainties are the standard deviation of the mean.)

The N_2O_5 and HNO_3 absorption bands are shown in Figure 4.

5. Nitrate Radical

The concentration of NO_3 was much too small to be accurately determined by the NO_x mass balance. Since the loss of two NO_3 molecules (reactions *g* and *B*) results in the production of approximately one N_2O_5 molecule, the NO_3 absorption cross section can be calculated from the ratio of modulation signals for N_2O_5 and NO_3. Both green and gold photolysis lamps were used in these measurements. Since the only quantity of interest in this part of the study was the ratio of modulation amplitudes, accurate values for the photon fluxes were not needed. The N_2O_5 modulation signal was averaged for 30 to 60 minutes at 1/4 cps, and the much stronger NO_3 signal for 10 minutes. The NO_3 modulation was monitored at 627 nm, the center of a fairly broad absorption band that obeyed Beer's law, and N_2O_5 was observed at its 8.03 μ infrared absorption peak. The stoichiometric factor (S.F.) relating the NO_3 and N_2O_5 concentration modulations was obtained for each set of conditions by a complete computer simulation. The NO_3 cross section at 627 nm could then be obtained from the N_2O_5 cross sections and the ratios of modulation amplitudes and optical path lengths:

$$\sigma_{627\ nm} = \sigma_{N_2O_5} \frac{1}{S.F.} \frac{A_{NO_3}}{A_{N_2O_5}} \frac{L_{N_2O_5}}{L_{NO_3}} \tag{25}$$

The averages from 24 sets of data[42] for Equation 25 are:

$$\begin{aligned} \sigma_{627}(298\ K) &= (7.03 \pm 0.18) \times 10^{-18}\ cm^2\ molecule^{-1} \\ \sigma_{627}(313\ K) &= (7.01 \pm 0.13) \times 10^{-18}\ cm^2\ molecule^{-1} \\ \sigma_{627}(329\ K) &= (7.04 \pm 0.13) \times 10^{-18}\ cm^2\ molecule^{-1} \end{aligned} \tag{26}$$

The absorption cross sections of NO_3 in this system, with corrections made for the visible ozone absorption, were averaged over each nm for presentation in Table II.

The average cross sections for NO_3 absorption for each lamp (red, gold, and green) were evaluated by Equation 20 over wavelength regions above and below 580 nm (the threshold for forming $NO_2 + O$) and entered in Table III with the average O_3 cross sections for each lamp.

B. Chemical Kinetic Data

1. N_2O_5 Catalyzed Decomposition of Ozone

Measurements of the N_2O_5 catalyzed decomposition of ozone were carried out using infrared scanning techniques for monitoring O_3, N_2O_5, and HNO_3. The reaction cell was conditioned with N_2O_5 and O_3 in a flow system at one atmosphere total pressure. The relative amount of N_2O_5 being converted to HNO_3 on the walls decreased slowly with time, but was always greater than 10 percent. When the flows were stopped, the N_2O_5 would be completely converted to nitric acid in 2 to 4 hours.

The reaction cell was closed off from the flow system at the start of an experiment. Ozone was measured by scanning the 4.4 to 5.76 μ region. Nitric acid and nitrogen pentoxide were then measured by scanning the 7.0 to 8.36 μ region. A set of measurements of all three species took 10 to 11 minutes. From 5 to 10 determinations of the concentrations of the three species were made over the course of an experiment by repeating the pair of scans as quickly as possible. The data points for each reactant were least-squares fitted to a third-order polynomial to give its concentration profile as a function of time. The decays of O_3 and N_2O_5 are illustrated by the profiles of concentration versus time presented in Figure 5. The polynomial curves for $[O_3]$ and $[N_2O_5]$ usually fit the data points with a standard deviation smaller than 0.2 percent. The differential rate of change of ozone was calculated from the concentration profile polynomials and used in Equation 7. The rate constants from the central portions of the curves were averaged and are presented in Table IV. The data were weighted by their standard deviations and least-squares fitted to Arrhenius parameters. The results for the two cells differed by 10 calories in the activation energy. The combined data give

$$\frac{1}{2}(Kh)^{2/3}(2g)^{1/3} = (1.39 \pm 0.19) \times 10^5 \, e^{-(9914 \pm 40)/T} \text{ cm molecules}^{-1/3} \text{ sec}^{-1} \quad (27)$$

The data from this work is compared to the results of Schumacher and Sprenger[18] on an Arrhenius plot in Figure 6.

2. NO_3 Steady State Concentrations

Nitrogen trioxide is a free radical intermediate in the N_2O_5–O_3 system, and its concentration depends on those of O_3 and N_2O_5 and on the rate constants relating the three species. The concentrations of NO_3, O_3, and N_2O_5 were measured under steady state flow conditions in the UV cell. The NO_3 visible absorption spectrum was scanned, and after a quick conversion of the system to infrared use, the N_2O_5 and O_3 spectra in the infrared were recorded. The NO_3 spectrum was then rescanned.

At three temperatures and over a wide range of concentrations of ozone and nitrogen pentoxide, a total of 136 determinations were made of the steady-state concentration of the NO_3 radical.[42] By means of successive approximations and the method of least squares, the quantities $Kh/2g$ and $w/2g$ of Equation 8 were evaluated. The results are summarized in Table V. The values for $(Kh/2g)^{1/3}$, weighted by their standard deviations, were fitted by the method of least squares to the Arrhenius equation to give

$$(Kh/2g)^{1/3} = (4.04 \pm 0.47) \times 10^{8} \exp(-3730 \pm 40)/T \qquad (28)$$

molecules$^{1/3}$ cm^{-1}, which is plotted in Figure 7. Schott and Davidson[4] measured the equilibrium constant K and the rate constant g at high temperature, Johnston and Yost[12] measured the rate constant h near room temperature, and the combined results from these studies for $(Kh/2g)^{1/3}$ are also shown in Figure 7. The present work differs from the older results by about a factor of three.

3. N_2O_5 Catalyzed Decomposition of Ozone with Photolytic Illumination of NO_3

Closed cell N_2O_5-O_3 decay experiments were also carried out with photolysis lamps flashing at 8 cps to obtain information on NO_3 photolysis products. Oxygen was used as the carrier gas to keep the steady state concentration of ozygen atoms low. The normal ozone decay could then be affected by reactions j_1 and j_2 for NO_3 photolysis and by reaction r, $O + O_2 + M$, if j_2 occurs. Experiments were performed in the UV cell using red, green, and gold lamps. The data were intially evaluated in Table VI using Equation 7, which does not take into account the effect of photolysis light in calculating the apparent rate constant for the N_2O_5 catalyzed decomposition of ozone. When the temperature of the system sometimes rose by 0.1 to 0.3 K due to heating by the lamps, the rate constants were extrapolated back to 297.8 K by Equation 27. Unilluminated experiments, performed in between the illuminated ones, gave rate constants within experimental error of the dark value predicted by Equation 27.

C. Modulation Experiments

The modulation experiments produced several types of kinetic information, including the identification of reaction species, the NO_3 visible absorption cross sections, the primary quantum yields for NO_3 photolysis, and the rate constants for oxygen atoms reacting with NO_3 and N_2O_5. All modulation experiments were performed in a flow system at one atmosphere total pressure.

1. Identification of Reaction Species

Preliminary experiments were carried out to determine the modulation behavior of the various reaction species. In the N_2O_5-O_3 flow system, the species present in significant concentrations were O_3, N_2O_5, HNO_3, and NO_3. The NO_3 modulation was monitored by its strong visible absorption spectrum. The amplitudes for different wavelengths in this spectrum were proportional to their respective NO_3 absorption cross sections, and the phase shifts were identical throughout the region. The NO_3 phase shifts for flashing frequencies near 1 cps were approximately 90°, indicating that NO_3 is a reactant being destroyed by light or fast intermediates. Ozone has a weak absorption that overlaps the NO_3 spectrum, but its predicted modulation amplitude was several orders of magnitude smaller than that of NO_3 and could not be detected at the visible, ultraviolet, or infrared ozone absorption bands.

The N_2O_5 modulation was monitored at its 8.03 μ infrared absorption peak. The phase shift for this signal always differed from that for NO_3 by approximately 180°, indicating that NO_3 and N_2O_5 have a reactant-product relationship. Modulation data were taken at 10 cm^{-1} intervals in the 1325 to 1375 cm^{-1} region where an NO_3 absorption band has been reported.[25] The NO_3 phase shift at 627 nm was 121°, and the N_2O_5 phase shift at 8.03 μ was -62°. The amplitude and phase shift data in Figure 8 indicate that this absorption band is due to N_2O_5. The absorption cross sections for this band were calculated from the 8.03 μ N_2O_5 cross section, and the ratio of modulation amplitudes are plotted in Figure 4.

Nitrogen dioxide was a low-concentration, fast intermediate in this system and attempts were made to detect this species by its strong near

ultraviolet absorption spectrum. Since no modulation signal could be detected, the ratio of the NO_3 concentration modulation to that for NO_2 was greater than a factor of 10, in agreement with computer simulations. Nitric oxide modulations in this system were much too small to be detected. The infrared absorption of HNO_3 at 7.70 μ was monitored to determine if nitric acid played a role in the modulation kinetics. Since no phase coherent signal was detected, the HNO_3 concentration modulation is at least a factor of 10 smaller than that of N_2O_5.

2. NO_3 Quantum Yields

According to Equation 19, the NO_3 modulation amplitude is directly proportional to its primary quantum yield. Modulation experiments were carried out to measure the quantum yield using red, green, and gold lamps. Oxygen was used as the carrier gas in order to suppress possible contributions to the modulation amplitude from oxygen atom reactions with NO_3 and N_2O_5. These experiments were performed in the UV reaction cell, and a summary of the data is presented in Table VII. The quantum yields were calculated from a computer simulation of the reaction system for each set of conditions. The light fluxes from Equation 21 and the absorption cross sections from Table III were used in the calculations. The variations in the observed quantum yields are mainly due to uncertainties in the light fluxes and to complications in the $[NO_3]$ determination: the green and gold lamps reduced the steady state concentration of NO_3 by 5 to 30 percent in the lighted portion of the reaction cell, but the optical path for spectroscopic monitoring also passed through the end caps (30 percent of the volume) where no NO_3 was photolyzed. Although

these two sections of the cell were treated separately in computations, convective mixing between the lighted and unlighted sections introduced noise into the modulation signal and some uncertainty into the NO_3 simulations.

3. Oxygen Atom Reactions

When nitrogen is substituted for the oxygen carrier gas (which had suppressed the oxygen atom concentration) the changes in modulation amplitudes can be attributed to reactions m and n. The primary quantum yields for NO_3 determined from the data in the previous section were used to calculate the NO_3 modulation amplitudes due to the photolysis reactions j_1 and j_2. The residual amplitudes observed with the nitrogen carrier gas were attributed to reactions m and n. Computer simulations showed a linear relationship between the rate constants m and n and the calculated modulation amplitudes due to these reactions. The modulation amplitudes for cases with N_2 as carrier gas are given in Table VIII.

V. Discussion

A. Absorption Cross Sections

The NO_3 cross sections presented in this work are about four times higher than previously reported values[23] since the earlier study used the values of K and g determined by Schott and Davidson[4] to calculate the steady state concentrations of NO_3. Schott and Davidson[4] extrapolated their 650 to 1050 K NO_3 cross sections determined in a shock tube to 300 K and obtained a value of 8.4×10^{-19} cm^2 $molecule^{-1}$ at 652 nm. The present study obtained a value of 3.9×10^{-19} cm^2 $molecule^{-1}$ at this wavelength and found an average overall increase in NO_3 cross sections with temperature (Table III). Since the wavelength chosen by Schott and Davidson lay between two strong absorption peaks, the possible variation in shape of both of these peaks with temperature made their long extrapolation uncertain.

The N_2O_5 ultraviolet cross sections in Table I are based on concentrations determined by infrared absorptions. These values supersede some earlier data[23] based on a fairly crude NO_x mass balance. The present results are up to 40 percent higher than those of Jones and Wulf[22] in the 290 to 310 nm region. The agreement is satisfactory, however, in view of the difficult experimental conditions in both studies.

The weak infrared abosrption band from 1325 to 1375 cm^{-1} attributed to NO_3 by Cramarossa and Johnston[25] has been identified by a molecular modulation study in this research as N_2O_5. Their study used long path infrared monitoring of the species in the N_2O_5-O_3 system and subtracted off a large overlying HNO_3 absorption. Part of their evidence for the band being NO_3 was an apparent one-third power dependence of the absorption

on the O_3 and N_2O_5 concentrations. The present experimental conditions gave NO_3 to N_2O_5 ratios similar to the earlier study, and a residual absorption was observed when the HNO_3 absorption was subtracted from the spectrum. The band was identified as N_2O_5 by its phase shift (Figure 8).

B. N_2O_5-O_3 Kinetics

The behavior of the N_2O_5-O_3 system in the unilluminated reaction cell can be well described by reactions *A* through *i* and *w*. The N_2O_5 catalyzed decomposition of ozone gave $\frac{1}{2}(Kh)^{2/3}(2g)^{1/3}$, Equation 27, and measurements of the steady state concentration of NO_3 as a function of N_2O_5 and O_3 led to $(Kh/2g)^{1/3}$, Equation 28. The equilibrium constant K was obtained by multiplying Equation 27 by 28 and dividing by the rate constant h. Substitution of K and h in Equation 27 or 28 then gave the rate constant g. These rate constants are listed in Table IX. The uncertainties for K and g were obtained by propagation of the standard deviations of h and of the quantities in Equations 27 and 28.

This rather involved method of obtaining values for K and g results in the accumulation of uncertainties from three different kinetic quantities. Equations 4 and 7 can be rearranged to give

$$\left(\frac{Kh}{2g}\right)^{1/3} = \frac{[NO_3]}{[O_3]^{1/3}[N_2O_5]^{1/3}\ \alpha^{1/3}} \tag{29}$$

$$(Kh)^{2/3}(2g)^{1/3} = \frac{-\frac{d[O_3]}{dt}}{[O_3]^{2/3}[N_2O_5]^{2/3}\ \alpha^{-1/3}} \tag{30}$$

Multiplying these two equations together and dividing by h, one finds

$$K = \frac{-\frac{d[O_3]}{dt}[NO_3]}{h[O_3][N_2O_5]} \tag{31}$$

The concentrations of chemical species in this expression were determined from experimentally measured absorption cross sections. Since the NO_3 cross section was derived experimentally as a direct multiple of that of N_2O_5, a systematic error in the N_2O_5 cross section would be canceled out. The ozone cross section is used in both the numerator and denominator, and the correction term for minor side reactions, α, cancels out in Equation 31. Hence, uncertainties in absorption cross sections should have little effect on the value obtained in this work for the equilibrium constant K.

The observed first-order loss of NO_3 in the dark was assumed to lead to NO_2 (reaction w) as a product in the proposed mechanism, but the possibility of NO (reaction w') being the product has not been eliminated. A chemiluminescence study of the NO_2-O_3 reaction indicated that no significant amount of NO was in the gas phase of this system. Even if the NO is formed heterogeneously, the effect is less than 0.2 percent in the values for $(Kh/2g)$ or $(w/2g)$ in Table V. The reaction w rate constants for the two sets of products are:

Temp (K)	w (sec^{-1})	w' (sec^{-1})
298	0.0026 ± 0.0003	0.0035 ± 0.0003
313	0.0031 ± 0.0005	0.0017 ± 0.0006
329	0.0055 ± 0.0020	0.006 ± 0.004

(32)

The enthalpy of formation of NO_3 can be obtained from the activation energy of the equilibrium constant K and the enthalpies of formation[54] of NO_2 and N_2O_5:

$$\Delta H_{f,300\ K.} = 17.6 \pm 0.2 \text{ kcal/mole} \qquad (33)$$

The calculated threshold wavelength for the photolysis of NO_3 to give NO_2 and $O(^3P)$ can then be calculated:

$$\Delta E_{300\ K} = 49.3 \pm 0.2 \text{ kcal/mole} \quad \text{and} \quad \lambda \leq 580 \pm 3 \text{ nm} \qquad (34)$$

The early study by Schumacher and Sprenger[18] of the N_2O_5 catalyzed decomposition of ozone used hundreds of torr of ozone and followed the reaction manometrically. The present research used only about three torr of ozone, but the measurements of $\frac{1}{2}(Kh)^{2/3}(2g)^{1/3}$ in the two systems agree within the experimental errors. The results from the present study have a higher precision, a larger temperature range, and both N_2O_5 and O_3 were directly measured by their infrared absorptions. The higher activation energy measured by Schumacher and Sprenger,[18] 20,700 calories versus 19,700 calories in the present study, could be due to reactant self-heating. The temperature rise in the present studies was calculated[55,56] to be less than 0.12 K, but the high concentrations of reactants in the earlier study would give a much larger rate of heat release.

The equilibrium constant K determined in this research has been used with literature data[3,6,10,36] to calculate rate constants for reactions *B*, *e*, and *f* (Table IX). In addition, the rate constants for the reaction of NO_3 with acetaldehyde and propylene measured by Morris and Niki[57] can be revised to give 1.7×10^{-15} cm^3 $molecule^{-1}$ sec^{-1} and 4×10^{-15} cm^3 $molecule^{-1}$ sec^{-1}, respectively.

C. NO_3 Photochemistry

The experimental data needed to determine the photochemistry of NO_3 are the observed quantum yields for NO_3 from molecular modulation studies in oxygen (Table VII) and the effect of illumination on the rate of the N_2O_5 catalyzed decomposition of ozone (Table VI). The two modes of photolysis of NO_3 have different effects on ozone. If the photolysis products are $NO_2 + O$, ozone is produced in an oxygen system via reaction r, $O + O_2 + M$. The primary quantum yield is the net effect observed on NO_3, and O_3 is formed:

$$\begin{array}{ll} NO_3 + h\nu \rightarrow NO_2 + O & (j_2) \\ O + O_2 + M \rightarrow O_3 + M & (r) \\ \hline \text{net:}\quad NO_3 + h\nu + O_2 \rightarrow NO_2 + O_3 & \end{array}$$

For photolysis of NO_3 giving a nitric oxide molecule that subsequently reacts with O_3, the observed quantum yield of NO_3 is the same as the primary quantum yield, and an O_3 molecule is destroyed:

$$\begin{array}{ll} NO_3 + h\nu \rightarrow NO + O_2 & (j_1) \\ NO + O_3 \rightarrow NO_2 + O_2 & (i) \\ \hline \text{net:}\quad NO_3 + h\nu + O_3 \rightarrow NO_2 + 2\ O_2 & \end{array}$$

If the NO reacts with NO_3, however, the observed quantum yield is twice the primary quantum yield, and O_3 is unaffected:

$$\begin{array}{ll} NO_3 + h\nu \rightarrow NO + O_2 & (j_1) \\ NO + NO_3 \rightarrow 2\ NO_2 & (f) \\ \hline \text{net:}\quad 2\ NO_3 + h\nu \rightarrow 2\ NO_2 + O_2 & \end{array}$$

The photolysis sources in this study were three broad-band fluorescent lamps with overlapping spectral distributions (Figure 2). In order to determine the products of NO_3 photolysis, the observed quantum yields in Table VII were combined with a detailed interpretation of the illuminated N_2O_5 catalyzed decomposition of ozone. The rate constants calculated by Equation 7 (no light reactions) for green and gold lamp illuminated experiments are listed in the first column of Table VI. (The quantum yields for red light photolysis were too small to yield information from this type of data treatment.) Rate constants were recalculated by Equation 12 for several possible distributions of products in an effort to obtain the expected $\frac{1}{2}(Kh)^{2/3}(2g)^{1/3}$ value (i.e., that given by Equation 27). The second set of values in Table VI takes into account the lowered steady state concentration of NO_3 due to photolysis, but does not make corrections for any ozone created or destroyed (i.e., j_1 and j_2 in the left-hand side of Equation 12 are zero). The next two columns of calculated rate constants contain ozone corrections and indicate the effects of attributing the observed quantum yield data of Table VII entirely to j_1 or j_2. The last column contains the quantum yields that result from fitting the data to the $\frac{1}{2}(Kh)^{2/3}(2g)^{1/3}$ value obtained in dark experiments (Equation 27). The quantum yields for green lamps in Table VII appear to be significantly lower at 329 K than at 298 K. The 329 K data was not as extensive as that at 298 K and was not used in the product analysis; the evidence for a temperature effect on the NO_3 quantum yield is not strong.

The quantum yields from the three sets of lamps at 298 K were used to estimate the wavelength dependence of photolysis products. Since

only broad bands of light were used in this study, the actual details of band shapes cannot be determined. Figure 9 presents one possible separation of the NO_3 spectrum into photochemically active bands. Since the red lamp quantum yields are so low, the strong 662 and 627 nm bands were assumed to be inactive. The red lamp intensity below 600 nm was quite small, and the red lamp quantum yield in Table VII was assumed to be due to reaction j_1. The distribution of light giving NO + O_2 as products was constrained by the very small overlap of the green and red lamp spectra (Figure 2) and the apparent values of j_1 for each lamp. Although the threshold energy for the formation of NO_2 and $O(^3P)$ was computed to be 580 ± 3 nm, vibrational and rotational energy could contribute to the dissociation process at higher wavelengths, as has been observed for NO_2.[58] In Table X, the products of average cross section and quantum yield deduced in Table VI from experimental results are compared with those calculated from the synthetic band shapes in Figure 9. Although the calculated j-values are all slightly lower than the experimental results, the values fall within the error limits of the measurements. The wavelength averaged NO_3 cross sections from Table III were used for the data analysis of Tables VI and X for convenience. The important photochemical parameter is the product of the quantum yield and absorption cross section, and although the data are consistent with any number of choices of quantum yield distributions and compatible cross sections different from Figure 9, the first-order photolysis rate constants would remain the same. In the 470 to 610 nm region, the average primary quantum yield was 0.23 for j_1 and 0.77 for j_2. The average quantum yield for j_1 in the strong 610 to 700 nm region was only 0.07.

Since the solar light flux from the green to red regions of the spectrum changes slowly with wavelength, the photolytic rates (cross section x light flux x quantum yield) calculated for NO_3 in the lower atmosphere have little dependence on the exact shape of the absorption bands that give the different products. Leighton[59] has tabulated solar light fluxes averaged over 100 Å intervals with corrections for ozone absorption, for the effects of particles in the atmosphere, and for Rayleigh scattering; these correction terms are not large in the region of the spectrum of the present work. The light fluxes for an overhead sun were used to calculate j-values:

$$j_1 = 0.040 \pm 0.02 \text{ sec}^{-1}$$
$$j_2 = 0.099 \pm 0.02 \text{ sec}^{-1}$$

The error limits are an estimate of the overall uncertainties in the component experiments. If the entire NO_3 visible absorption band was photochemically active, the total j-value would be 0.27 sec^{-1}.

The NO_3 free radical is important in several gas phase reaction mechanisms, but little is known about its structure or electronic states. Walsh[60] predicted that the molecule has D_{3h} symmetry and a $^2A_2'$ ground electronic state. Semi-empirical calculations by Olsen and Burnelle,[61] however, predict a Y-shaped structure with a $^2B_2$ ground state. Although the nitrate anion has absorptions in the 1350 to 1400 cm^{-1} and 720 to 830 cm^{-1} regions,[62] no infrared absorption bands for the NO_3 free radical have been observed.

Several reactions are energetically possible in the region of the strong NO_3 visible absorption spectrum:

$$NO_3 + h\nu \rightarrow NO + O_2(^3\Sigma_g^-) \qquad \lambda \leq 8\ \mu$$

$$\rightarrow NO + O_2(^1\Delta_g) \qquad \lambda \leq 1100\ nm$$

$$\rightarrow NO + O_2(^1\Sigma_g^+) \qquad \lambda \leq 700\ nm$$

$$\rightarrow NO_2 + O(^3P) \qquad \lambda \leq 580\ nm$$

The quantum yield results of this research indicate that both NO and NO_2 are formed by NO_3 photolysis, but the electronic states of the products were not identified.

The extremely strong NO_3 absorption bands at 662 and 627 nm are the first two transitions in a series that Ramsey[24] identified as involving symmetric stretching vibrations. The results obtained here indicate that absorption of light at these wavelengths does not lead to photolysis of NO_3 at a total pressure of one atmosphere. Collisional deactivation appears to be faster than dissociation to NO + O_2 when NO_3 is excited in these bands. Whether NO_3 has a symmetrical D_{3h} structure or a Y-shaped C_{2v} structure, the "reaction coordinate" to form NO + O_2 does not have the symmetry of a symmetric stretch, but more nearly that of an anti-symmetric stretch. Although the other bands of NO_3 have not been interpreted, it is tempting to speculate that absorption in anti-symmetric bands leads to NO + O_2. Below 580 nm, the primary quantum yield seems to be close to unity. If NO_3 is Y-shaped, the symmetric-stretching normal coordinate would have a large component of bond-breaking to give an oxygen atom.

These results indicate a substantial amount of formation of NO_2 + O at wavelengths above the 580 nm threshold (Figure 9). This effect could be the participation of rotational energy in the bond-breaking process.

However, an analysis of the energy present from the Boltzmann distributions of rotational and vibrational levels for a D_{3h} structure showed that it could account for only 40 percent of the effect shown in Figure 9. This discrepancy may reflect a partial failure of this method to separate j_1 and j_2. These results clearly point out the need for further experimentation: (1) using monochromatic radiation, (2) varying the wavelength, (3) varying total pressure at each wavelength, and (4) some variation of temperature.

D. Oxygen Atom Reactions

The interpretation of the rate data for the reactions of N_2O_5 and NO_3 with oxygen atoms (reactions *m* and *n*, respectively) is highly dependent on the other kinetic parameters measured in this study. When the oxygen carrier gas was replaced by nitrogen, there was a change in the NO_3 molecular modulation amplitude as shown in Table VIII. Computer simulations were carried out using the entire mechanism plus various assumed values for the rate constants *m* and *n*. For reaction *m* the effect on the observed NO_3 modulation amplitude is of opposite sign depending on products:

$$N_2O_5 + O \rightarrow 2\ NO_3 \qquad (m')$$

$$N_2O_5 + O \rightarrow 2\ NO_2 + O_2 \qquad (m'')$$

The experimental data yield the result that the absolute value of the difference in m' and m'' is $\leq 2 \times 10^{-14}$ cm^3 $molecule^{-1}$ sec^{-1} at 298 K; this was determined by the absence of any identifiable effect and the sensitivity of the method. Within experimental error the value of the rate constant *n* was the same at 298 and 329 K:

$$n = (1.0 \pm 0.4) \times 10^{-11} \text{ cm}^3 \text{ molecules sec}^{-1}$$

This value is fairly close to that for the similar reaction of atomic oxygen with nitrogen dioxide,[37] which is 9.1×10^{-12} cm^3 molecule^{-1} sec^{-1}.

E. Check on Mechanism and Rate Constants

The molecular modulation data at a flashing frequency of 1/4 cps have been used, along with other data, to evaluate some of the rate constants in Table IX. A check on the consistency of the procedure was to use the mechanism and rate constants to predict the modulation amplitude and phase shift for NO_3 at other flashing frequencies. A series of experiments was conducted with the gold colored lamps flashing at frequencies between 1/4 and 8 cps with $[O_3] = 6.2 \times 10^{16}$, $[N_2O_5] = 1.22 \times 10^{15}$, $[O_2] = 2.46 \times 10^{19}$, $[NO_3] = 5.4 \times 10^{13}$ molecules cm^{-3}, and T = 298 K. The experimental and calculated amplitudes and phase shifts are plotted in Figure 10. A similar set of experiments was carried out using the green colored lamps at 329 K with $[O_3] = 2.4 \times 10^{16}$, $[N_2O_5] = 7.5 \times 10^{14}$, $[O_2] = 2.23 \times 10^{19}$, and $[NO_3] = 11.6 \times 10^{13}$; calculated and observed results are plotted in Figure 11. Within experimental error the observed data agree with the calculated amplitudes and phase shifts, and provide a partial confirmation of the mechanism and rate constants described by this study.

F. Errors

These studies were carried out with well-defined experimental conditions and with primary spectroscopic data having a precision of

one percent or better. Water vapor adsorbed by the cell's walls converted nitrogen pentoxide to nitric acid, and the HNO_3 concentration was from 10 to 20 percent of that of N_2O_5 in the flow experiments. Although no significant reactions of nitric acid with O_3, O, or NO_3 are known, there is some uncertainty as to whether the ever-present nitric acid was undergoing an unrecognized chemical reaction. The separation of quantum yields of NO_3 for the two sets of products depended on small perturbations of kinetic data by NO_3 irradiation, and the non-illuminated ends of the reaction cell introduced uncertainty in the average concentration of NO_3 being photolyzed. The wavelength resolution of the quantum yield was only approximate due to the broad-band nature of the fluorescent lamp spectra, but this should not cause a major error in the photolysis rate constants for atmospheric conditions. Finally, the rate constants m and n are derived from the five to ten percent difference between two large numbers, and these rate constants had all the accumulated errors of the entire study.

Acknowledgment

This work was supported in part by the National Science Foundation Grant No. CHE-75-17833, by the Materials and Molecular Research Division of the Lawrence Berkeley Laboratory, and by the Climatic Impact Assessment Program.

Work performed under the auspices of the U. S. Energy Research and Development Administration.

References

1. H. S. Johnston, J. Am. Chem. Soc. 73, 4542 (1951).
2. F. Daniels and E. H. Johnston, J. Am. Chem. Soc. 43, 53 (1921).
3. H. S. Johnston and Yu-sheng Tao, J. Am. Chem. Soc. 73, 2948 (1951).
4. G. Schott and N. Davidson, J. Am. Chem. Soc. 80, 1841 (1958).
5. J. H. Smith and F. Daniels, J. Am. Chem. Soc. 69, 1735 (1947).
6. R. L. Mills and H. S. Johnston, J. Am. Chem. Soc. 73, 938 (1951).
7. H. S. Johnston and R. L. Perrine, J. Am. Chem. Soc. 73, 4782 (1951).
8. H. S. Johnston, J. Am. Chem. Soc. 75, 1567 (1953).
9. D. J. Wilson and H. S. Johnston, J. Am. Chem. Soc. 75, 5763 (1953).
10. R. L. Mills, Ph.D. Thesis, Standord University, 1951.
11. I. C. Hisatsune, B. Crawford, Jr., and R. A. Ogg, Jr., J. Am. Chem. Soc. 79, 4648 (1957).
12. H. S. Johnston and D. M. Yost, J. Chem. Phys. 17, 386 (1949).
13. C. H. Wu, E. D. Morris, Jr., and H. Niki, J. Phys. Chem. 77, 2507 (1973).
14. R. A. Graham and H. S. Johnston, J. Chem. Phys. 60, 4628 (1974).
15. D. D. Davis, J. Prusazcyk, M. Dwyer, and P. Kim, J. Phys. Chem. 78, 1775 (1974).
16. J. T. Herron and R. E. Huie, Int. J. Mass Spectrom. Ion Physics 16, 125 (1975).
17. G. Sprenger, Z. Elektrochem. 37, 674 (1931).
18. H. J. Schumacher and G. Sprenger, Z. Physik. Chem. 2B, 266 (1929).
19. M. E. Nordberg, Science 70, 580 (1929).
20. T. M. Lowry and R. V. Seddon, J. Chem. Soc., 1461 (1938).

21. H. S. Johnston, Science 173, 517 (1971).

22. E. J. Jones and O. R. Wulf, J. Chem. Phys. 5, 873 (1937).

23. H. S. Johnston and R. Graham, Can. J. Chem. 52, 1415 (1974).

24. D. A. Ramsay, Proc. Colloq. Spectroscopy Int., 10th, 583 (1962).

25. F. Cramarossa and H. S. Johnston, J. Chem. Phys. 43, 727 (1965).

26. R. Dalmon, Mem. Serv. chim. etat. 30, 141 (1943).

27. S. C. Schmidt, R. C. Amme, D. G. Murcray, A. Goldman, and F. S. Bonomo, Nature (London), Phys. Sci. 238, 109 (1972).

28. H. S. Johnston and R. Graham, J. Phys. Chem. 77, 62 (1973).

29. F. Biaume, J. Photochem. 2, 139 (1973/74).

30. G. S. Beddard, D. J. Giachardi, and R. P. Wayne, J. Photochem. 3, 321 (1974/75).

31. D. G. Murcray, T. G. Kyle, F. M. Murcray, and W. J. Williams, J. Opt. Soc. Am. 59, 1131 (1969).

32. D. G. Murcray, A. Goldman, A. Csoeke-Poeckh, F. H. Murcray, W. J. Williams, and R. N. Stocker, J. Geophys. Res. 78, 7033 (1973).

33. R. F. Murphy, Ph.D. Thesis, University of California, Los Angeles, 1969.

34. H. S. Johnston, Gas Phase Reaction Rate Theory, Ronald Press Co., New York, 1966, pp. 14-32.

35. S. W. Benson, The Foundations of Chemical Kinetics, McGraw-Hill Book Co., Inc., New York, 1960, pp. 408-418.

36. A. B. Harker and H. S. Johnston, J. Phys. Chem. 73, 1153 (1973).

37. D. Garvin and R. F. Hampson, Editors, Chemical Kinetics Data Survey, NBSIR 74-430, 1974.

38. A. C. Hindmarsh, Lawrence Livermore Laboratory Report UCID-30001, Rev., 1, 1972.

39. A. B. Harker, Ph.D. Thesis, University of California, Berkeley, 1972.

40. E. D. Morris, Jr., Ph.D. Thesis, University of California, Berkeley, 1968.

41. E. D. Morris, Jr. and H. S. Johnston, Rev. Sci. Instrum. 39, 620 (1968).

42. R. A. Graham, Ph.D. Thesis, University of California, Berkeley, 1975.

43. G. Z. Whitten, "Rate Constant Evaluations Using a New Computer Modeling Scheme," paper presented at ACS National Meeting (Spring, 1974).

44. G. A. W. Rutgers and J. C. DeVos, Physics XX, 715 (1954).

45. J. C. DeVos, Physics XX, 690 (1954).

46. E. Castellano and H. S. Schumacher, J. Chem. Phys. 36, 2238 (1962).

47. E. Castellano and H. S. Schumacher, Z. Physik. Chem. 34, 198 (1962).

48. M. Griggs, J. Chem. Phys. 49, 857 (1968).

49. A. P. Altshuller, J. Phys. Chem. 61, 251 (1957).

50. D. M. Waldorf and E. L. Balb, J. Chem. Phys. 39, 432 (1963).

51. R. A. Cox and R. G. Derwent, J. Photochem. 6, 23 (1976/77).

52. A. M. Bass, A. E. Ledford, Jr., and A. H. Laufer, J. Res. Natl. Bur. Stand. 80A, 143 (1976).

53. E. D. Morris, Jr. and H. Niki, J. Phys. Chem. 77, 1929 (1973).

54. D. D. Wagman, W. H. Evans, V. B. Parker, I. Halow, S. M. Bailey, and R. H. Schumm, NBS Technical Note 270-3 (1968).

55. T. Boddington and D. Gray, Proc. Roy. Soc. London A. 320, 71 (1970).

56. P. G. Ashmore, B. J. Tyler and T. A. B. Wesley, 11th Int. Symp. on Combustion, 1133 (1967).

57. E. D. Morris, Jr. and H. Niki, J. Phys. Chem. 78, 1337 (1974).

58. J. N. Pitts, Jr., J. H. Sharp, and S. I. Chan, J. Chem. Phys. 42, 3655 (1964).

59. P. A. Leighton, Photochemistry of Air Pollution, Academic Press, New York, 1961, pp. 26-71.

60. A. D. Walsh, J. Chem. Soc., 2306 (1953).

61. J. F. Olsen and L. Burnelle, J. Am. Chem. Soc. 92, 3659 (1970).

62. K. Nakamoto, Infrared Spectra of Inorganic and Coordinations Compounds, John Wiley & Sons, Inc., New York, 1963, p. 92.

Figure Captions

Figure 1. Schematic diagram of experimental apparatus.

Figure 2. Relative intensities of photolysis lamps at 298 K and absorption spectra of NO_3 and ozone. The dashed vertical line is the threshold for formation of NO_2 + O from the photolysis of NO_3.

Figure 3. Nitrogen pentoxide (N_2O_5) ultraviolet spectrum at 298 K.

Figure 4. Nitrogen pentoxide and nitric acid (dashed line) infrared spectra at 298 K.

Figure 5. An example of concentration profiles for N_2O_5-O_3 static cell decay.

Figure 6. Arrhenius plot for $\frac{1}{2}(Kh)^{2/3}(2g)^{1/3}$.

Figure 7. Arrhenius plot for $\left(\frac{Kh}{2g}\right)^{1/3}$.

Figure 8. Modulation amplitude and phase shifts for the 1320 to 1380 cm^{-1} region at 329 K with green lamps.

Figure 9. Separation of the NO_3 spectrum into photochemically active bands with synthetic shapes.

Figure Captions (continued)

Figure 10. Modulation amplitudes and phase shifts of NO_3 for gold lamp photolysis at 298 K.

Figure 11. Modulation amplitudes and phase shifts of NO_3 for green lamp photolysis at 329 K.

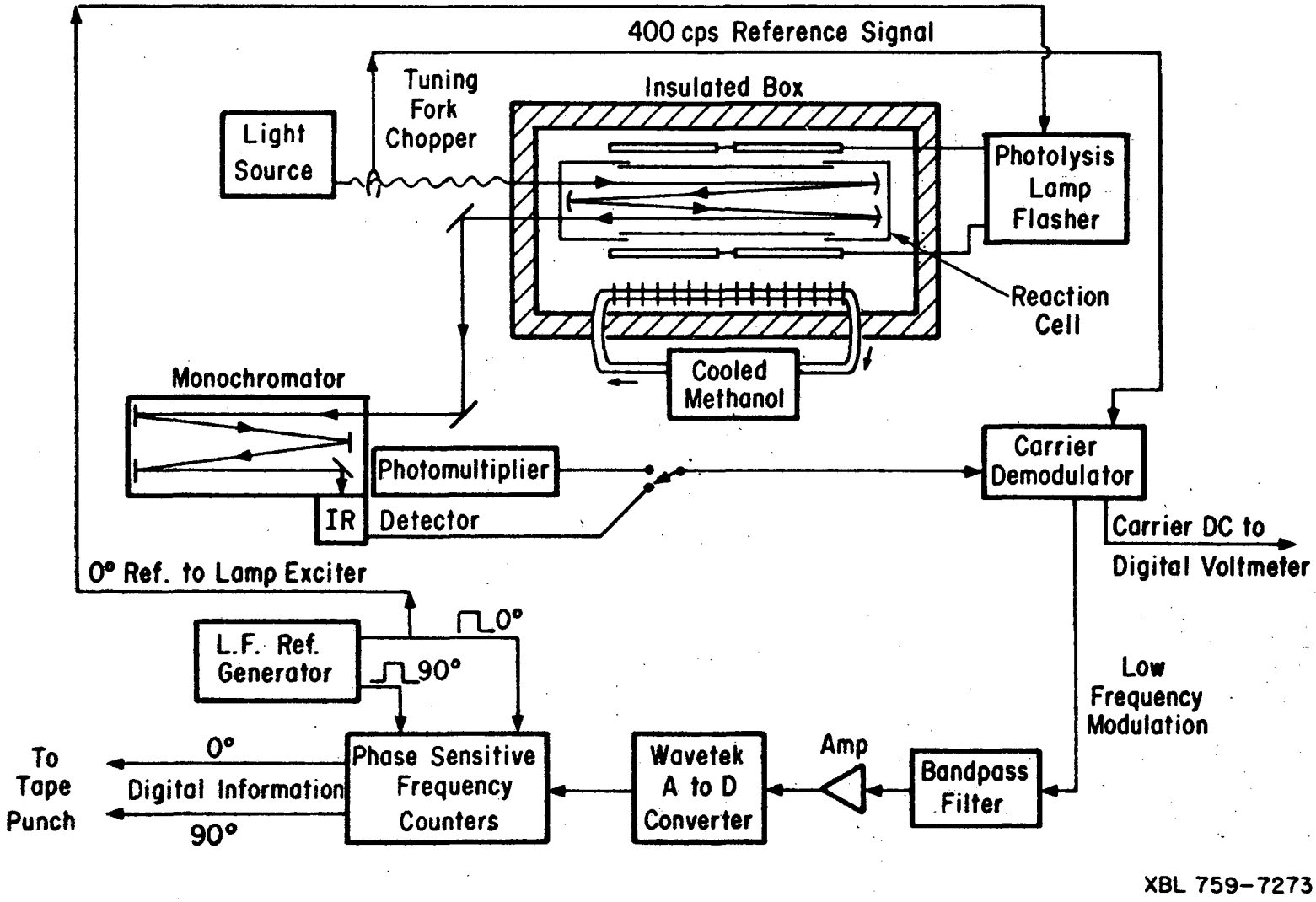
400 cps Reference Signal
Tuning Fork Chopper
Insulated Box
Light Source
Photolysis Lamp Flasher
Reaction Cell
Cooled Methanol
Monochromator
Photomultiplier
IR Detector
Carrier Demodulator
Carrier DC to Digital Voltmeter
0° Ref. to Lamp Exciter
L.F. Ref. Generator
0°
90°
Low Frequency Modulation
To Tape Punch
0°
Digital Information
90°
Phase Sensitive Frequency Counters
Wavetek A to D Converter
Amp
Bandpass Filter
XBL 759-7273

Fig. 1

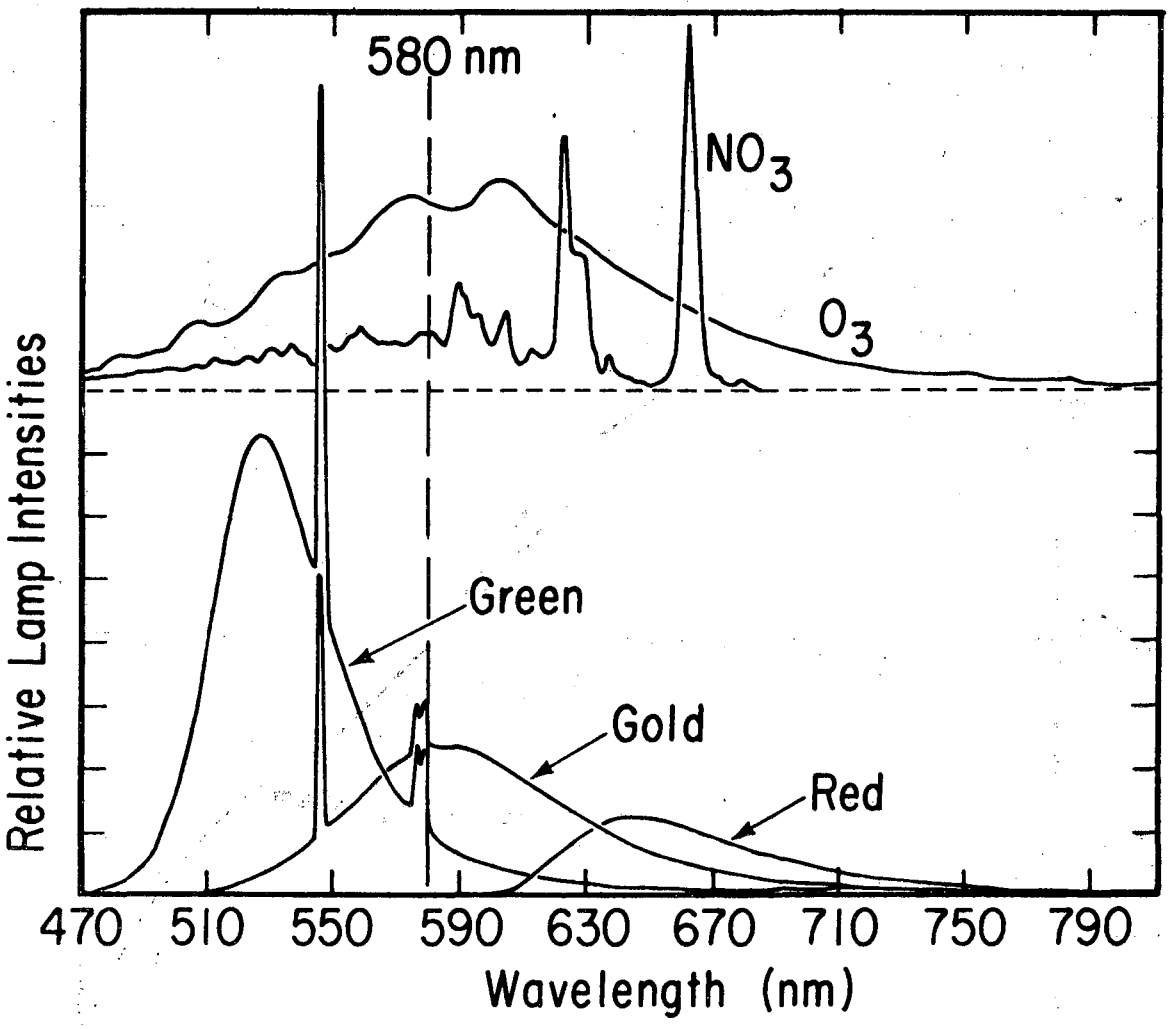

XBL 759-7285

Fig. 2

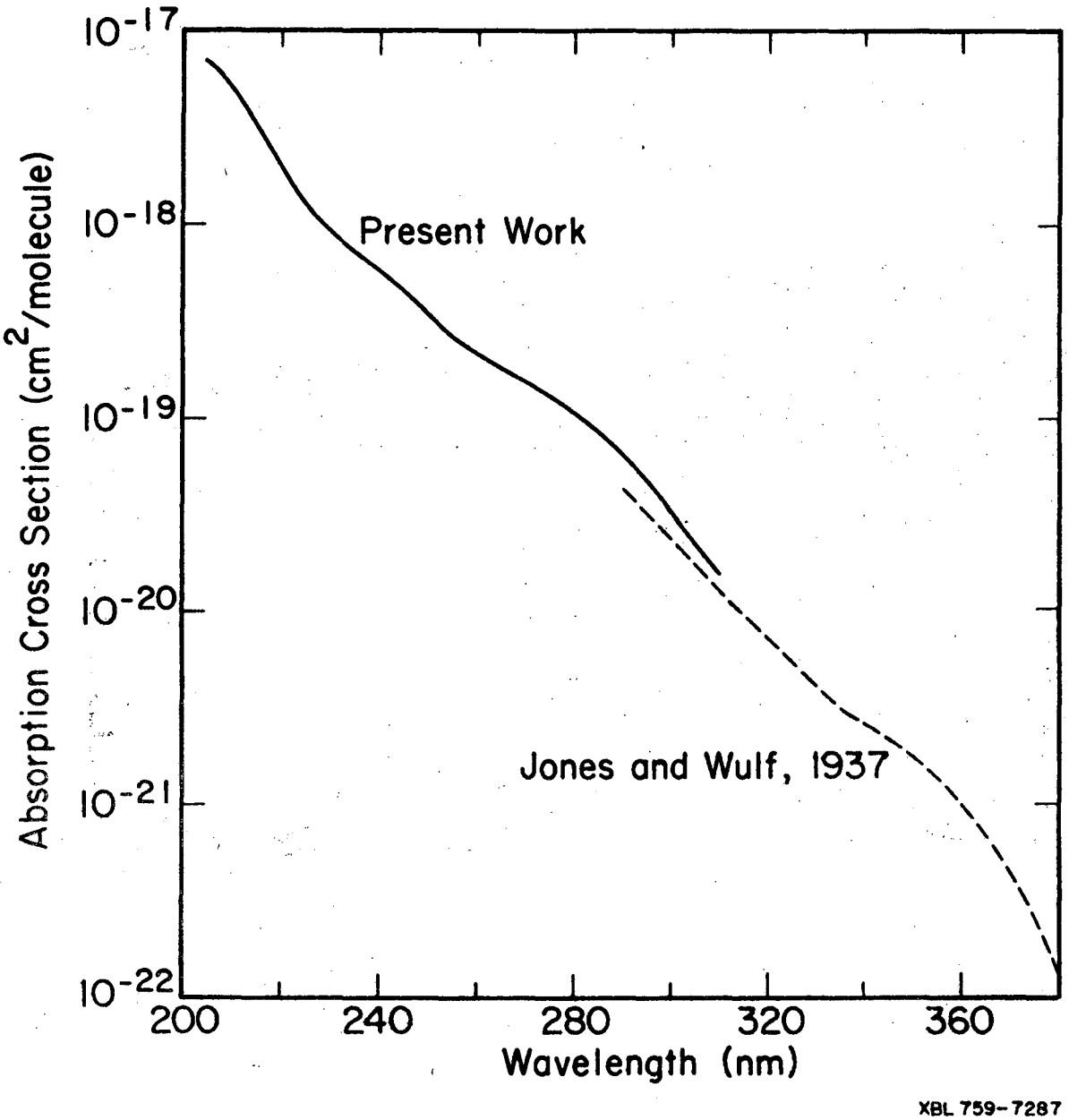
Absorption Cross Section (cm²/molecule)
10⁻¹⁷
10⁻¹⁸
10⁻¹⁹
10⁻²⁰
10⁻²¹
10⁻²²
Present Work
Jones and Wulf, 1937
200
240
280
320
360
Wavelength (nm)
XBL 759-7287

Fig. 3

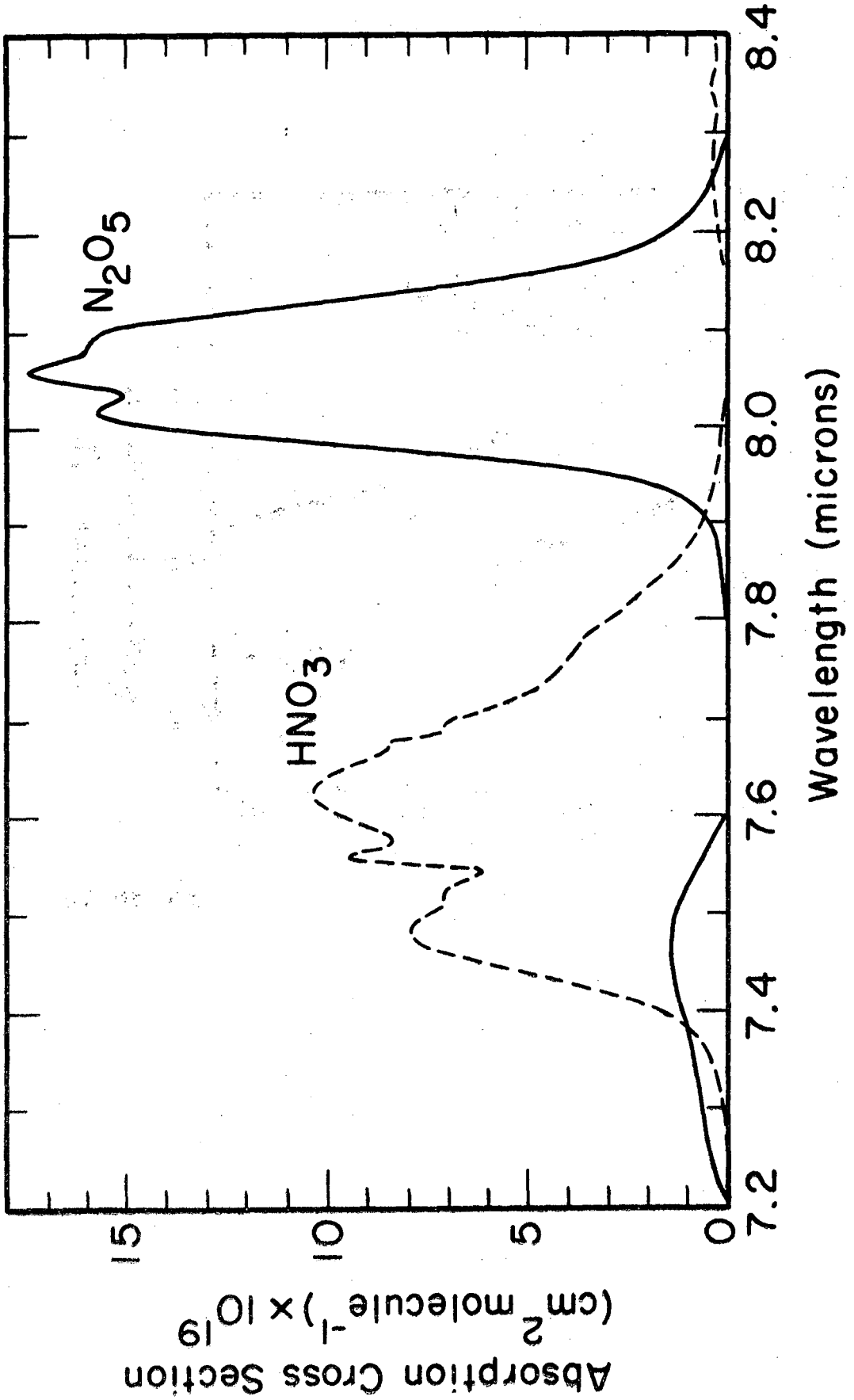
Absorption Cross Section
(cm² molecule⁻¹) × 10¹⁹
15
10
5
0
7.2
7.4
7.6
7.8
8.0
8.2
8.4
Wavelength (microns)
N2O5
HNO3

Fig. 4

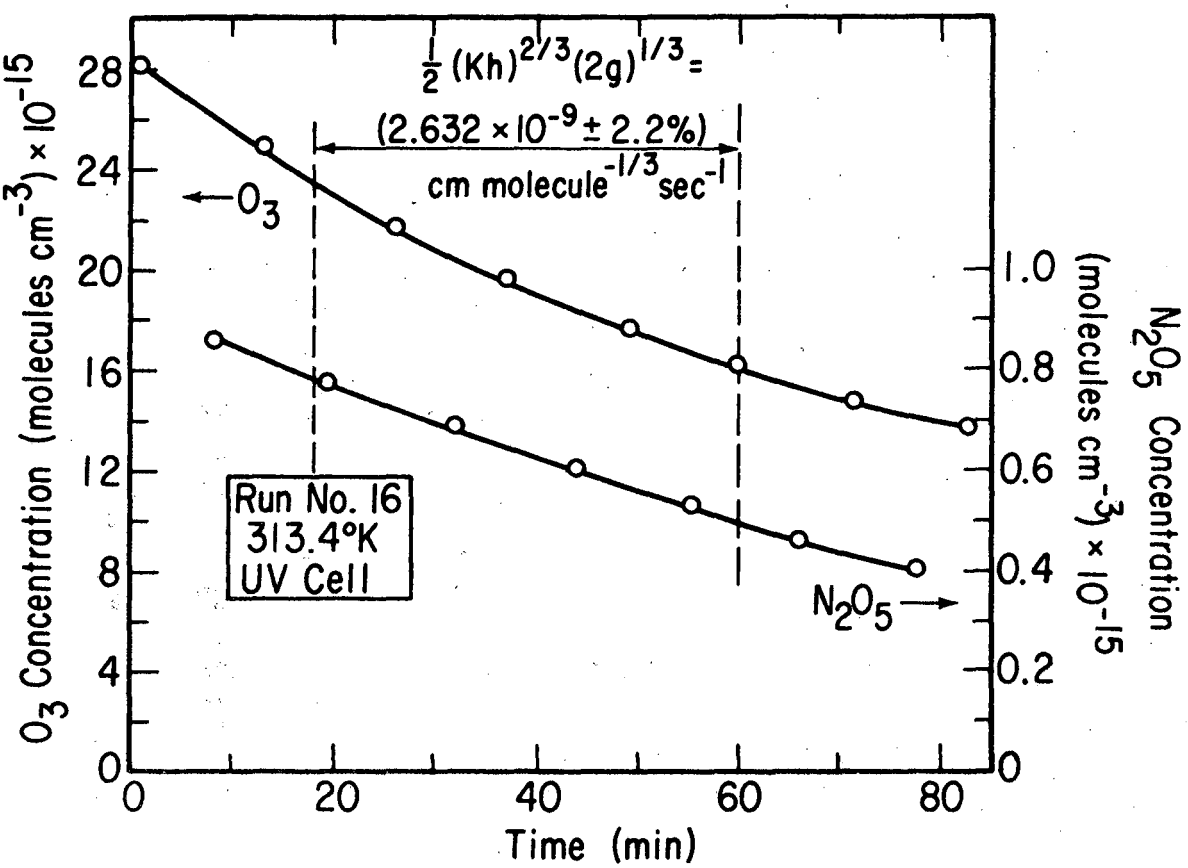

XBL 759-7288

Fig. 5

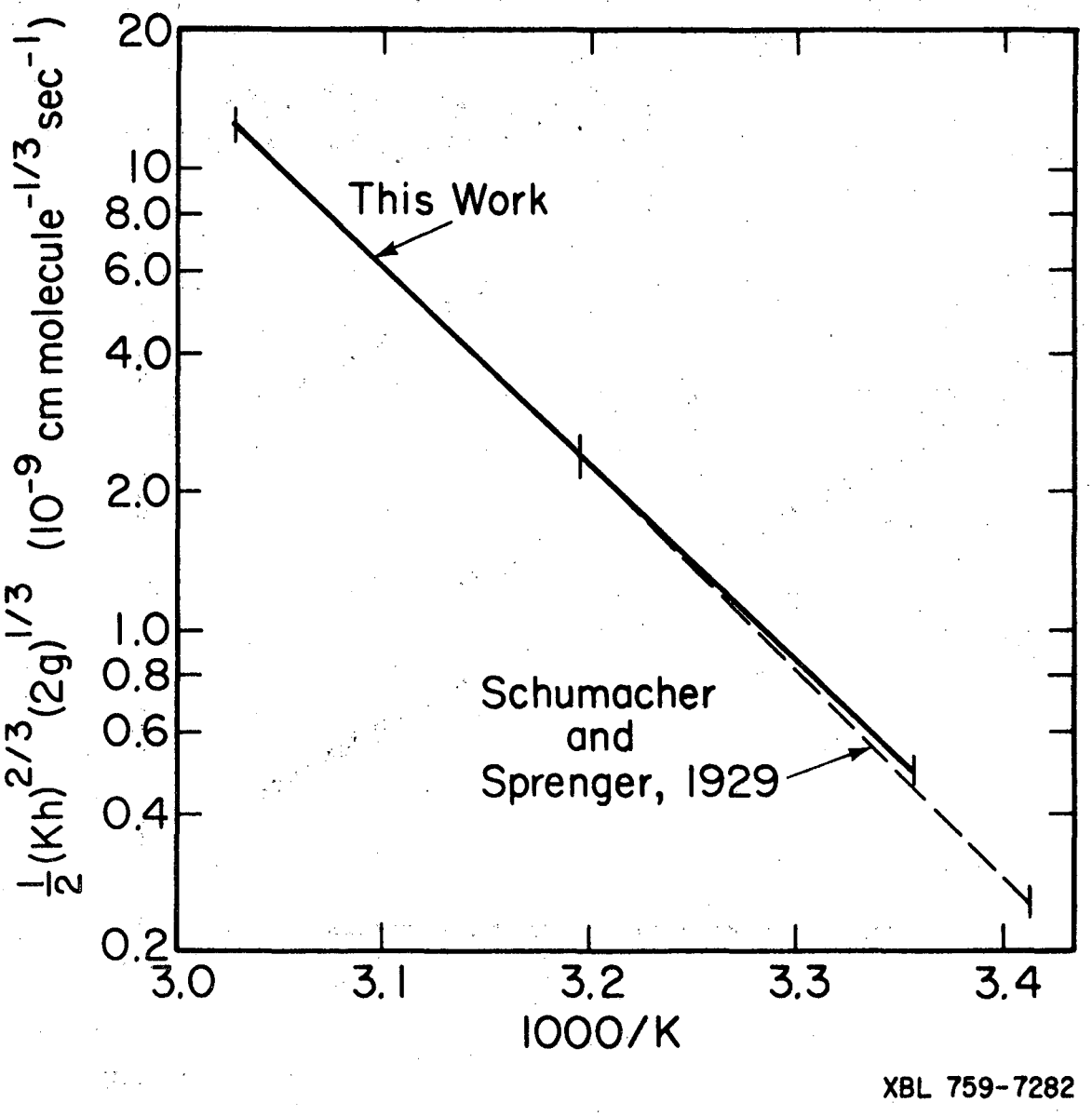

Fig. 6

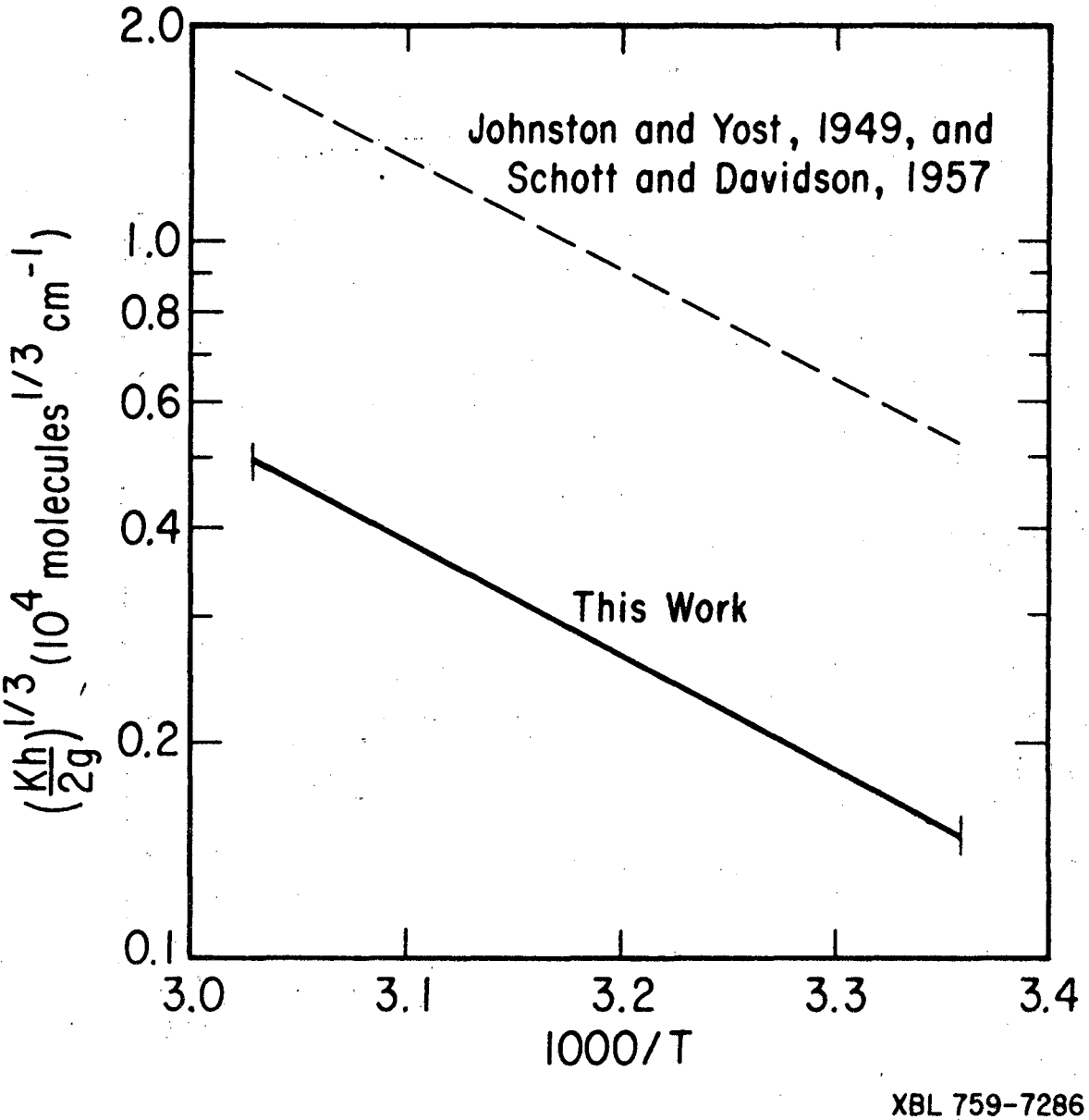
2.0
1.0
0.8
0.6
0.4
0.2
0.1
3.0
3.1
3.2
3.3
3.4
1000/T
Johnston and Yost, 1949, and
Schott and Davidson, 1957
This Work
$(\frac{Kh}{2g})^{1/3}(10^4 \text{ molecules}^{1/3} \text{ cm}^{-1})$
XBL 759-7286

Fig. 7

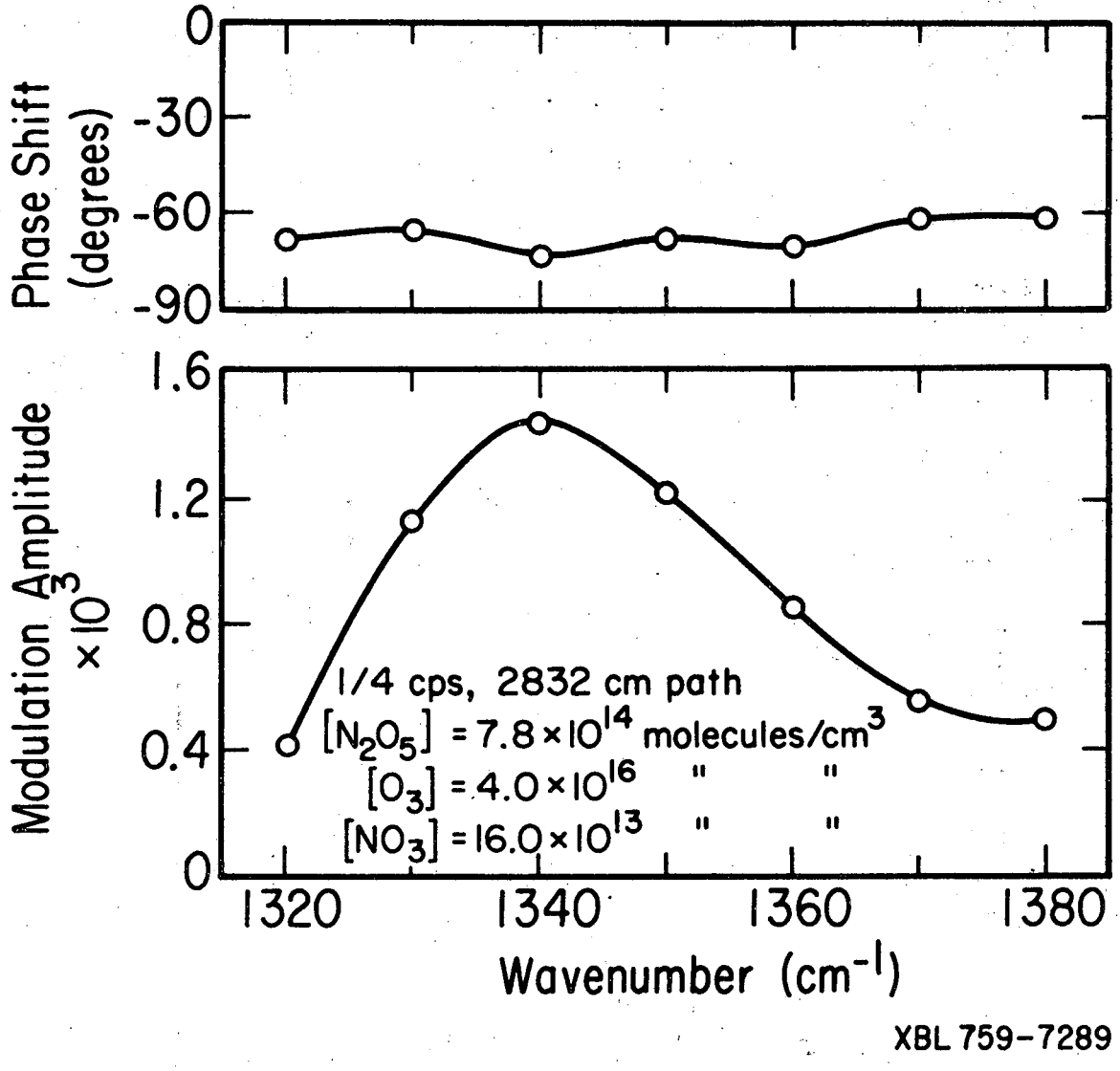

Fig. 8

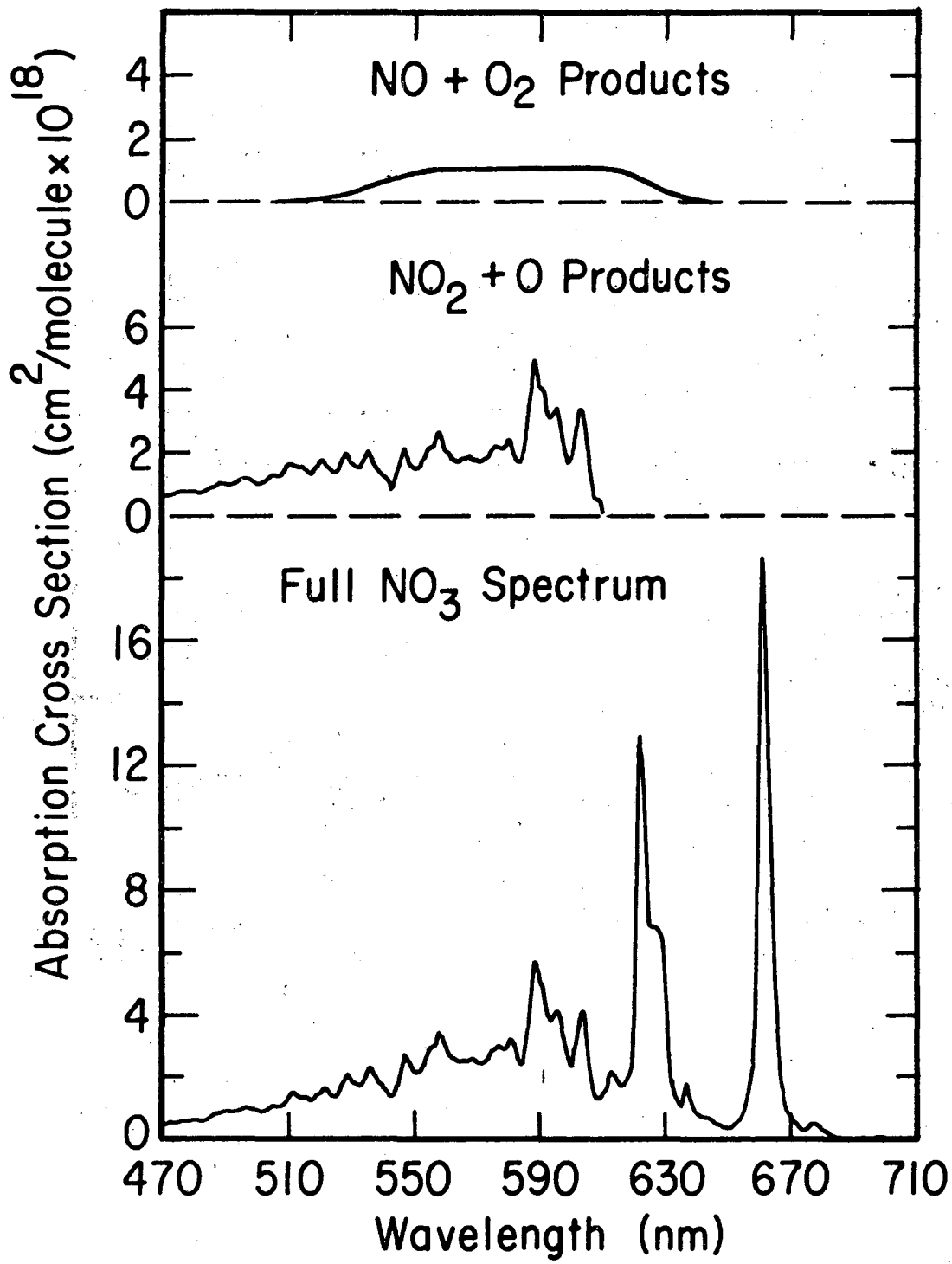

XBL 759-7290

Fig. 9

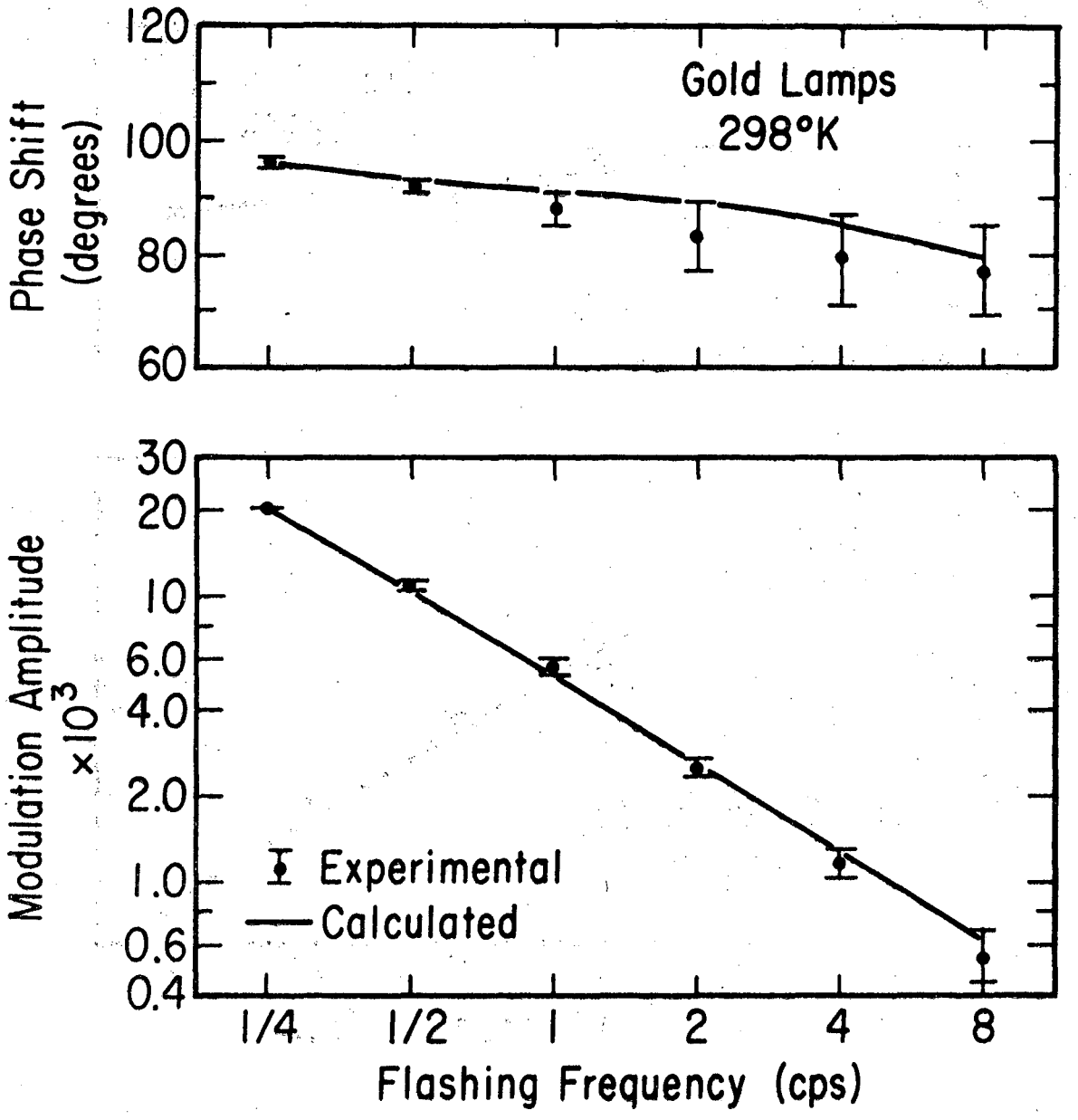

XBL 7510-7468

Fig. 10

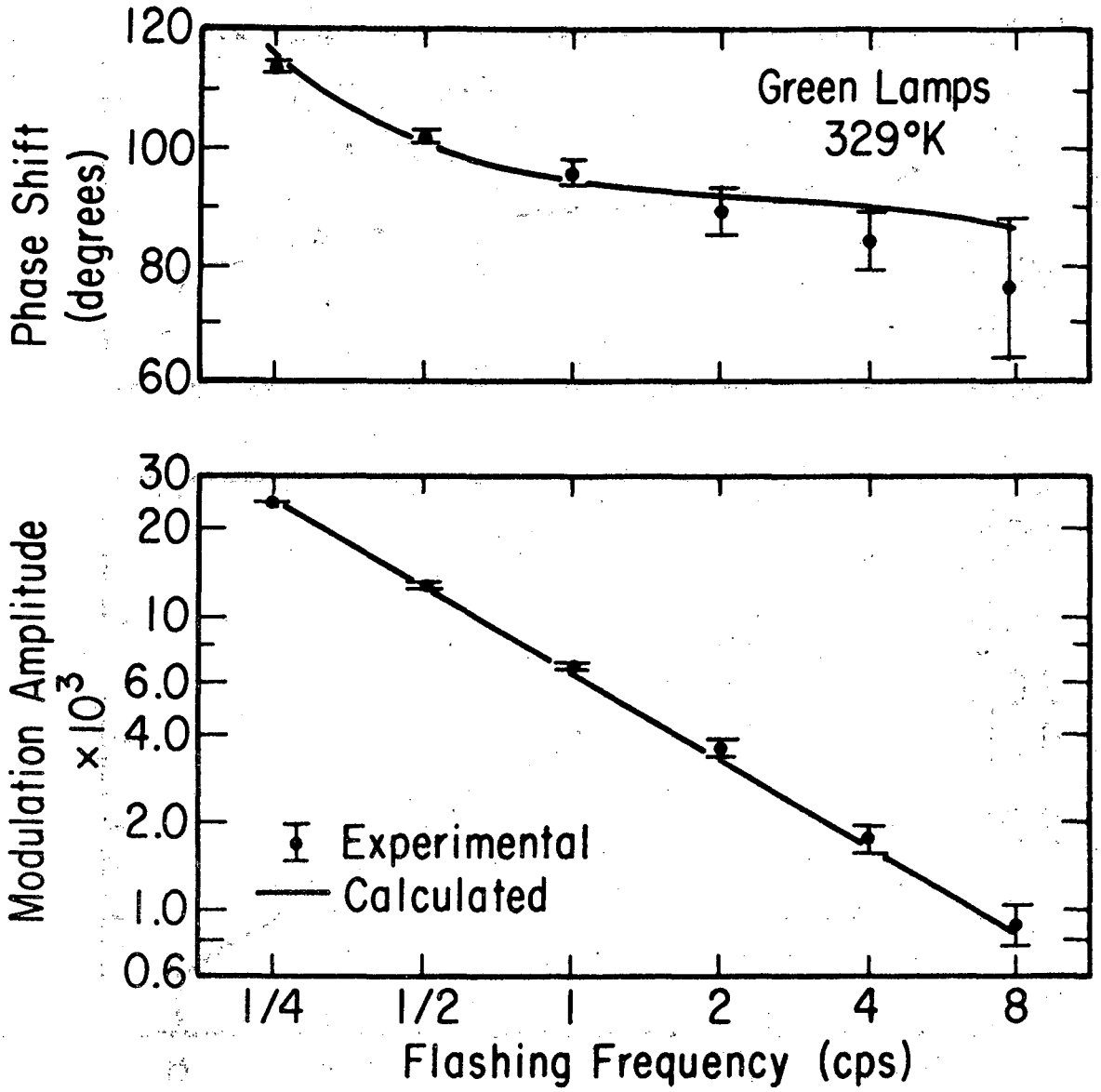

XBL 759-7291

Fig. 11

Table I. Ultraviolet absorption cross sections for N_2O_5 at 298 K

Present Work				Jones and Wulf (ref. 22)	
λ nm	$10^{19}\sigma$ cm^2	λ nm	$10^{19}\sigma$ cm^2	λ nm	$10^{19}\sigma$ cm^2
205	69	265	1.77	290	0.42
210	52	270	1.52	300	0.24
215	33	275	1.25	310	0.13
220	20.6	280	1.07	320	0.075
225	13.1	285	0.83	330	0.040
230	9.3	290	0.63	340	0.027
235	7.2	295	0.46	350	0.018
240	5.7	300	0.32	360	0.010
245	4.5	305	0.22	370	0.0047
250	3.5	310	0.15	380	0.0013
255	2.63				
260	2.12				

Table II. Absorption cross sections (cm^2 $molecule^{-1}$, base e) averaged over each nm for the nitrogen trioxide (NO_3) free radical at 298 K

λ	$10^{19}\sigma$	λ	$10^{19}\sigma$	λ	$10^{19}\sigma$	λ	$10^{19}\sigma$	λ	$10^{19}\sigma$	λ	$10^{19}\sigma$
400	0.0	456	3.2	512	16.1	568	25.7	624	116.6	680	4.9
401	0.1	457	3.4	513	15.1	569	26.3	625	86.5	681	3.5
402	0.1	458	3.7	514	14.1	570	25.3	626	70.0	682	2.5
403	0.3	459	3.9	515	14.0	571	25.1	627	69.0	683	1.6
404	0.2	460	3.9	516	14.0	572	24.8	628	68.9	684	0.9
405	0.5	461	3.6	517	13.0	573	24.7	629	67.0	685	0.5
406	0.3	462	3.5	518	12.1	574	25.5	630	64.1	686	0.3
407	0.1	463	3.8	519	12.8	575	27.0	631	50.2	687	0.2
408	0.3	464	4.1	520	14.4	576	29.2	632	32.7	688	0.4
409	0.5	465	4.5	521	15.8	577	30.5	633	19.9	689	0.2
410	0.6	466	4.5	522	17.2	578	30.3	634	13.2	690	0.1
411	0.5	467	4.8	523	16.6	579	29.4	635	10.6	691	0.0
412	0.3	468	5.0	524	15.0	580	29.9	636	12.3	692	0.0
413	0.7	469	5.2	525	13.8	581	32.0	637	16.4	693	0.1
414	0.7	470	4.9	526	13.7	582	31.0	638	17.6	694	0.1
415	0.6	471	5.0	527	15.1	583	26.8	639	13.4	695	0.2
416	0.3	472	5.4	528	17.9	584	24.7	640	9.8	696	0.4
417	0.4	473	5.5	529	21.0	585	24.6	641	7.8	697	0.4
418	0.6	474	5.6	530	20.9	586	27.5	642	6.8	698	0.4
419	0.9	475	5.9	531	19.1	587	34.8	643	6.9	699	0.4
420	0.9	476	6.4	532	18.1	588	44.8	644	7.1	700	0.3
421	0.9	477	6.8	533	17.3	589	55.2	645	6.7	701	0.2
422	0.8	478	6.6	534	17.7	590	56.7	646	5.6	702	0.2
423	1.0	479	6.4	535	20.2	591	51.9	647	4.9	703	0.1
424	1.2	480	6.4	536	23.2	592	48.3	648	4.8	704	0.0
425	1.3	481	6.5	537	23.8	593	43.2	649	3.7		
426	0.9	482	6.3	538	21.1	594	39.2	650	3.2		
427	0.8	483	6.1	539	18.8	595	39.1	651	3.3		
428	1.2	484	6.2	540	18.1	596	41.6	652	3.9		
429	1.2	485	6.6	541	16.8	597	40.9	653	4.7		
430	1.2	486	7.4	542	16.8	598	35.4	654	5.7		
431	1.5	487	8.0	543	14.3	599	28.9	655	6.9		
432	1.4	488	8.0	544	13.9	600	24.5	656	8.9		
433	1.5	489	8.6	545	16.2	601	24.5	657	11.8		
434	1.7	490	9.3	546	20.4	602	28.4	658	16.8		
435	2.1	491	9.2	547	25.6	603	33.9	659	27.6		
436	2.1	492	8.9	548	27.5	604	40.0	660	51.2		
437	1.8	493	8.9	549	24.9	605	41.8	661	101.5		
438	1.8	494	8.8	550	22.4	606	33.8	662	170.8		
439	2.1	495	9.1	551	21.4	607	23.2	663	170.4		
440	1.9	496	10.4	552	21.6	606	15.9	664	115.4		
441	1.9	497	11.2	553	22.2	609	13.3	665	73.5		
442	2.0	498	10.8	554	24.5	610	13.5	666	48.6		
443	1.9	499	10.3	555	27.8	611	14.3	667	29.7		
444	2.1	500	9.8	556	29.5	612	16.9	668	17.5		
445	2.3	501	9.4	557	30.0	613	21.7	669	10.7		
446	2.3	502	9.1	558	31.7	614	22.4	670	7.5		
447	2.5	503	9.5	559	34.3	615	19.9	671	6.0		
448	2.8	504	10.5	560	32.3	616	17.4	672	5.7		
449	2.8	505	11.6	561	28.5	617	16.7	673	4.7		
450	2.7	506	11.9	562	26.8	618	18.3	674	3.6		
451	2.8	507	11.4	563	25.9	619	20.2	675	3.0		
452	3.1	508	10.6	564	24.8	620	24.7	676	3.1		
453	3.2	509	11.2	565	24.7	621	39.8	677	4.0		
454	3.4	510	13.0	566	25.8	622	76.1	678	5.5		
455	3.5	511	15.1	567	25.5	623	120.4	679	5.9		

Table III. Wavelength averaged cross sections (cm^2 $molecule^{-1}$) of NO_3 and O_3 for different photolysis lamps

	Lamp	σ_{NO_3} ($\lambda \leq 580$ nm)	% Light	σ_{NO_3} ($\lambda > 580$ nm)	% Light	σ_{O_3}
298 K	Green	1.88×10^{-18}	93	2.99×10^{-18}	7	2.76×10^{-21}
	Gold	2.51×10^{-18}	37	3.11×10^{-18}	63	3.82×10^{-21}
	Red	-	0	2.12×10^{-18}	100	2.13×10^{-21}
329 K	Green	2.01×10^{-18}	93	3.10×10^{-18}	7	2.76×10^{-21}
	Gold	2.67×10^{-18}	37	3.22×10^{-18}	63	3.82×10^{-21}
	Red	-	0	2.17×10^{-18}	100	2.13×10^{-21}

Table IV. N_2O_5 catalyzed decomposition of ozone

Run No.	Temp (K)	$[O_3]_o$ (10^{15} molec/cm^3)	$[N_2O_5]_o$	$\frac{1}{2}(Kh)^{2/3}(2g)^{1/3}$ (10^{-9} cm molec$^{-1/3}$ sec^{-1})	% Stan. Dev.
		(IR Cell: Surface/Volume = .180 cm^{-1})			
1	298.8	29.0	2.03	0.547	1.6
2	298.8	72.6	1.40	0.561	1.7
3	298.8	63.7	1.09	0.547	0.8
4	314.4	55.3	0.96	2.972	2.3
5	314.4	43.8	1.23	2.891	1.1
6	314.4	38.7	1.71	2.808	1.5
7	330.2	21.9	0.42	12.41	5.4
8	330.2	9.31	0.31	12.31	4.1
		(UV Cell: Surface/Volume = .252 cm^{-1})			
9	297.8	53.3	0.58	0.488	1.9
10	297.8	58.8	1.07	0.482	1.2
11	297.8	67.4	1.38	0.462	1.5
12	297.8	31.7	1.28	0.504	2.6
13	297.9	85.1	1.10	0.499	2.2
14	297.9	40.4	0.56	0.479	1.8
15	313.4	30.1	0.67	2.558	3.5
16	313.4	23.6	0.79	2.632	2.2
17	313.4	31.2	0.76	2.597	1.9
18	329.0	39.0	0.25	10.99	2.7
19	329.0	29.2	0.45	10.82	4.4
20	329.0	31.4	0.83	11.09	4.1

Table V. Summary of $[NO_3]_{ss}$ data

Temp (K)	No. of Obs.	$[O_3]$ Range (10^{16})	$[N_2O_5]$ Range (10^{14})	$[NO_3]$ Range (10^{13})	$\frac{Kh}{2g}$	$\frac{w}{2g}$
		(molecules cm^{-3})			(10^{10} molecules cm^{-3})	(10^{13} molecules cm^{-3})
297.8	62	0.6 - 11	0.5 - 14	1.0 - 7.6	0.3127 ± 0.0059	0.573 ± 0.056
313.4	41	0.2 - 7	0.7 - 15	1.5 - 13	2.018 ± 0.034	0.454 ± 0.071
329.0	33	1.5 - 7	1.4 - 7	6.0 - 16	11.16 ± 0.39	1.12 ± 0.39

Table VI. Calculation of $1/2(Kh)^{2/3}(2g)^{1/3}$ for the illuminated reaction cell with all temperatures corrected to 297.8 K

Run No.	Lamps	$1/2(Kh)^{2/3}(2g)^{1/3}$ (10^{-9} cm molecule$^{-1/3}$ sec^{-1}) (No j_1 and j_2 Corrections)	$1/2(Kh)^{2/3}(2g)^{1/3}$ (10^{-9} cm molecule$^{-1/3}$ sec^{-1}) ($[NO_3]_{ss}$ Corrections Only)	$1/2(Kh)^{2/3}(2g)^{1/3}$ (10^{-9} cm molecule$^{-1/3}$ sec^{-1}) (All j_1)	$1/2(Kh)^{2/3}(2g)^{1/3}$ (10^{-9} cm molecule$^{-1/3}$ sec^{-1}) (All j_2)	$1/2(Kh)^{2/3}(2g)^{1/3}$ (10^{-9} cm molecule$^{-1/3}$ sec^{-1}) (Fitted to give 0.484)	
24	Green	0.422	0.371	0.312	0.520	j_1 = .11 j_2 = .90	j_1: 0.14 ± 0.06 (σ_{avg} = 2.99 x 10^{-18} cm^2 molecule^{-1})
26	Green	0.440	0.396	0.344	0.535	j_1 = .17 j_2 = .80	j_2: 0.85 ± 0.10 (σ_{avg} = 1.88 x 10^{-18} cm^2 molecule^{-1})
27	Gold	0.478	0.430	0.396	0.529	j_1 = .25 j_2 = .60	j_1: 0.23 ± 0.04 (σ_{avg} = 3.11 x 10^{-18} cm^2 molecule^{-1})
29	Gold	0.472	0.423	0.391	0.524	j_1 = .23 j_2 = .62	
30	Gold	0.468	0.429	0.387	0.521	j_1 = .20 j_2 = .66	j_2: 0.63 ± 0.06 (σ_{avg} = 2.51 x 10^{-18} cm^2 molecule^{-1})

Table VII. Observed quantum yields for NO_3 photolysis from 1/4 cps modulation data

Lamps	Temp (K)	$[NO_3] \times 10^{-13}$	$[N_2O_5] \times 10^{-14}$	$[O_3] \times 10^{-16}$	L (cm)	Mod. Amp. (@ 627 nm)	Observed Q.Y.
		(molecules cm^{-3})					
Red	298	6.00	11.19	6.076	1416	.00046	.084
	298	2.274	3.22	1.157	2832	.00034	.085
	298	5.33	13.62	3.364	1416	.00033	.071
Red	329	12.04	8.38	2.045	1416	.00067	.078
	329	13.70	16.97	1.545	1416	.00077	.084
Green	298	2.74	3.96	3.11	708	.00518	1.11
	298	4.00	8.65	3.434	708	.00740	1.06
	298	5.25	11.00	5.94	708	.01002	1.08
	298	5.02	5.96	9.35	708	.00914	1.03
Green	329	14.71	5.07	6.35	708	.0267	.80
	329	11.22	2.64	5.48	708	.0218	.86
	329	7.35	4.15	1.120	708	.01336	.80
	329	11.49	7.19	2.40	708	.01991	.77
	329	17.49	14.85	3.86	708	.02800	.75
Gold	298	5.49	11.41	6.12	1416	.01757	1.03
	298	5.58	11.86	6.17	1416	.01775	1.04
	298	3.656	15.24	1.607	1416	.01144	1.06
	298	3.645	15.16	1.583	1416	.01154	1.08
	298	5.71	12.66	6.27	1416	.01824	1.04
	298	5.83	13.09	6.32	1416	.01855	1.04

Table VIII. NO_3 modulation amplitude with N_2 as principal carrier gas and difference between these cases with N_2 and corresponding cases with O_2 as carrier gas

Temp (K)	Concentrations (molecules cm^{-3} x 10^{-14})		Modulation Amplitude x 10^3	
	$[N_2O_5]$	$[NO_3]$	Observed	Difference
298	15.45	0.333	12.98	1.01
	7.78	0.270	10.41	0.86
	2.96	0.195	7.26	0.57
329	12.03	1.225	28.30	3.65
	4.85	0.991	23.71	3.06
	1.87	0.753	18.51	2.62

Table IX. Rate constants and NO_3 photolysis constants for eleven reactions in the mechanism, as derived from the literature or obtained in this work

Quantity	T Range of Observations	A-factor (cm^3 sec^{-1} unless noted)	E_a (degrees K)	Ref
A (1 atm)	273 - 300	1.24×10^{14} sec^{-1}	10,317	6,10
Ke	338 - 396	2.05×10^{13} sec^{-1}	12,406	3
Kf	297	(0.71 ± 0.014)		36
K	298 - 329	$(8.4 \pm 1.8) \times 10^{26}$ cm^{-3}	11178 ± 100	*
B (1 atm)	273 - 300	$(1.48 \pm 0.33) \times 10^{-13}$	-861 ± 300	A/K
e	338 - 396	$(2.5 \pm 0.5) \times 10^{-14}$	1127 ± 100	Ke/K
f	297	$(1.87 \pm 0.41) \times 10^{-11}$		36
g	298 - 329	$(8.5 \pm 2.8) \times 10^{-13}$	2450 ± 100	*
h	231 - 298	$(1.34 \pm 0.11) \times 10^{-13}$	2466 ± 30	14
i	198 - 330	$(9. \times 10^{-13})$	1200	37
j_1	Sunlight	(0.040 ± 0.02) sec^{-1}		*
j_2	Sunlight	(0.099 ± 0.02) sec^{-1}		*
m	298	$\leq 2 \times 10^{-14}$		*
n	298 - 329	$(1.0 \pm 0.4) \times 10^{-11}$	0	*
q	220 - 1000	1.9×10^{-11}	2300	37
r	200 - 346	6.6×10^{-35} cm^6 sec^{-1} (M: Ar = 1.0, N_2 = 1.6, O_2 = 1.7)	-510	37

*This work.
Error limits are based on random errors of this study and do not include possible systematic errors.

Table X. Comparison of experimental results with the synthetic spectra of Figure 9

(σ_{avg} in units of 10^{-18} cm^2 $molecule^{-1}$)

j_1: $NO + O_2$	Experimental Results			Calculated Results		
	Green	Gold	Red	Green	Gold	Red
ϕ	0.14 ± .06	0.23 ± .04	0.049 ± .010			
σ_{avg}	2.99	3.11	2.17			
$\phi\ \sigma_{avg}$	0.42 ± .13	0.71 ± .05	0.11 ± .02	0.40	0.67	0.10
j_2: $NO_2 + O$						
ϕ	0.85 ± .10	0.63 ± .06	-			
σ_{avg}	1.88	2.51	-			
$\phi\ \sigma_{avg}$	1.60 ± .10	1.58 ± .15	-	1.50	1.40	-

This report was done with support from the United States Energy Research and Development Administration. Any conclusions or opinions expressed in this report represent solely those of the author(s) and not necessarily those of The Regents of the University of California, the Lawrence Berkeley Laboratory or the United States Energy Research and Development Administration.

TECHNICAL INFORMATION DIVISION
LAWRENCE BERKELEY LABORATORY
UNIVERSITY OF CALIFORNIA
BERKELEY, CALIFORNIA 94720